THE UNIVERSITY *of* EDINBURGH

# Edinburgh Research Explorer

# Constraints on the rates of degassing and convection in basaltic open-vent volcanoes

**Citation for published version:**
Palma, JL, Blake, S & Calder, ES 2011, 'Constraints on the rates of degassing and convection in basaltic open-vent volcanoes' Geochemistry, Geophysics, Geosystems, vol 12, no. 11, Q11006., 10.1029/2011GC003715

**Digital Object Identifier (DOI):**
10.1029/2011GC003715

**Link:**
Link to publication record in Edinburgh Research Explorer

**Document Version:**
Publisher final version (usually the publisher pdf)

**Published In:**
Geochemistry, Geophysics, Geosystems

OPEN ACCESS

Geochemistry
Geophysics
Geosystems

G³

# Constraints on the rates of degassing and convection in basaltic open-vent volcanoes

**José L. Palma**

*Center for Geohazards Studies, State University of New York at Buffalo, 411 Cooke Hall, Buffalo, New York 14260-1350, USA (josepalm@buffalo.edu)*

*Department of Earth and Environmental Sciences, Open University, Walton Hall, Milton Keynes MK7 6AA, UK*

**Stephen Blake**

*Department of Earth and Environmental Sciences, Open University, Walton Hall, Milton Keynes MK7 6AA, UK*

**Eliza S. Calder**

*Department of Geology, State University of New York at Buffalo, 411 Cooke Hall, Buffalo, New York 14260-1350, USA*

[1] Variations in gas emissions of open-vent volcanoes are investigated using a model of magma convection in narrow conduits. Laboratory experiments with both vertical and inclined conduits and dimensional analysis show that for Grashof numbers lower than 100 the volumetric rate of magma ascent is a simple function of equivalent conduit radius, density difference between the magmas, and viscosity of the degassed magma that descends back to the reservoir. The rate of magma ascent depends on the *flux coefficient*, estimated as 0.1 and 0.2 for vertical and inclined conduits, respectively. The *equivalent radius* parameter accounts for the dimensions of the conduit(s) regardless of its geometry, thus extending the treatment by previous models that used flow in pipes. The volume flow rate of convection increases with higher density difference and conduit size, but is also highly influenced by the large variations in viscosity of the degassed magma as volatile content and crystallinity change. The model presented here can be used to constrain the degassing and ascent rates of volatile-rich magma when combined with petrologic data on magmatic volatile content. Application of the model to Villarrica volcano (Chile) reveals that the background degassing levels observed (~3 kg s$^{-1}$ SO$_2$) are associated with convective ascent of a relatively degassed magma (0.04 wt% S, ~0.5 wt% H$_2$O), while episodes of higher SO$_2$ emissions (measurements up to 15 kg s$^{-1}$) can be explained by the ascent of magma with higher volatile content (up to 0.09 wt% S, ~1.5 wt% H$_2$O).

# 1. Introduction

[2] Basaltic volcanic systems are characterized by long narrow feeding conduits within which magma ascends from a deep source to the surface driven primarily by buoyancy [*Turcotte*, 1987; *Corsaro and Pompilio*, 2004; *Cigolini et al.*, 2008]. In these systems, degassing, crystallization and cooling of magma generate density gradients within the conduit system and hence cause natural convection driven by buoyancy contrasts. At persistently degassing volcanoes such as Stromboli, Villarrica, Mt. Etna, Mt. Erebus, Ambrym and Masaya, convection of magma within their plumbing system is inferred to explain the imbalance between the large volumes of magma degassed and the small volume of magma erupted [*Kazahaya et al.*, 1994; *Stevenson and Blake*, 1998; *Shinohara*, 2008]. Although magma convection in the conduit has been accepted as a viable mechanism for persistent degassing associated with low extrusion rates [e.g., *Wallace and Anderson*, 1998; *Sparks*, 2003; *Locke et al.*, 2003; *Stix*, 2007; *Burton et al.*, 2007a; *Oppenheimer et al.*, 2009], the fluid mechanics of magma convection in the plumbing system and its consequences on the rate and style of degassing activity observed at the vent are not well understood. In particular, there is incomplete knowledge about the three-dimensional flow regimes, and in fact a variety of configurations are plausible, such as core-annular flow, stratified flow, slug flow, helical flow, or turbulent flow [e.g., *Arakeri et al.*, 2000; *Debacq et al.*, 2003; *Mandal et al.*, 2007; *Huppert and Hallworth*, 2007]. Furthermore, the effects of inclining the pipe from vertical and the effect of a dike-shaped conduit rather than a cylindrical conduit are not well constrained even though they are likely components of natural systems.

[3] This paper investigates the convective flow in narrow conduits, and its consequences on the variable degassing rates of open-vent systems through theoretical and experimental analysis of convection in both vertical and inclined pipes, thus extending the work of *Stevenson and Blake* [1998] and *Huppert and Hallworth* [2007] (where only vertical pipes were considered). In the experiments the convection is driven by the density difference between two fluids in two chambers that are connected by a pipe. We investigate vertical and tilted tubes and the resulting flow configurations which are more variable than those in previous studies, and we extend the theory of countercurrent flow in a pipe to that of a slot or dike configuration.

The concept of *equivalent conduit radius* is introduced in the treatment, which is then valid for any plumbing system and eliminates having to make assumptions about plumbing geometry. A measure of the dimensions of the plumbing system is also introduced which can be used to investigate changes in observed volcanic activity determined by variations in the initial gas content of fresh magma entering the conduit.

[4] The following section describes some theoretical aspects of open-system degassing and constraints on magma flow in narrow conduits. Section 3 then describes the laboratory experiments and the parametric description of their results. In Section 4 we combine petrologic data, measurements of gas emissions, and the conclusions of Sections 2 and 3, in order to constrain magma degassing in open systems with specific application of the model to Villarrica volcano, Chile. An appendix presents the model of core-annular flow in a cylindrical pipe and a slot.

# 2. Magma Flow in Open Systems

## 2.1. Magma Degassing

[5] Open-system degassing typically involves (1) the transport of volatile-bearing magmas from deep levels in the crust toward relatively shallow levels where the gas can reach supersaturation, (2) diffusion and exsolution of gas, and (3) outgassing through hydrothermal systems, conduit walls, open vents, etc. Here, magma degassing refers to the exsolution of gas from the melt, gas segregation and outgassing, whereas the term outgassing refers only to the escape of gas from the magma. In order to fully understand the characteristics of magma degassing, it is necessary to analyze the conditions under which this fresh magma ascends within the plumbing system of the volcano, its interaction with more evolved and perhaps degassed magma, and the flow regime of the two-phase magma (melt and gas) within the conduit(s).

[6] A schematic of magma degassing in an open-vent basaltic system is depicted in Figure 1. In this model it is assumed that most of the gas escapes at the vent. At depths where most of the gas is still dissolved in the melt, volatile-bearing magma is transported toward the surface while degassed magma sinks. In this part of the system convection of magmas is assumed to occur. The widespread assumption in such cases is that one of these magmas ascends from deeper levels and is more
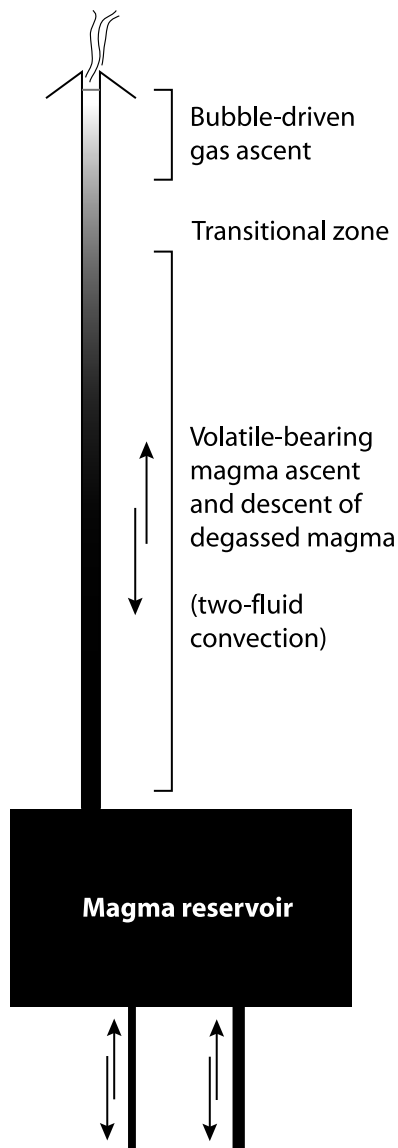
**Figure 1.** Conceptual model of magma transport and degassing in low-silica open-vent volcanoes. In the upper part of the plumbing system, a few kilometers long, gas-bearing magma rises in two separate regimes. At depth, a two-magma convection develops where the fraction of volatiles exsolved is minimum and the gas-phase speed is much lower than the magma ascent speed. Above this zone, increasing exsolution of volatiles and bubble growth driven by decompression transforms the dynamics of magma ascent into a two-phase flow regime. Note that in this regime the convection of degassed and partly degassed magma still exist. If the magma reservoir is open to new inputs of fresh magma from deeper levels, the two-magma convection can also in theory exist below this magma chamber. In this figure, the scale of grey indicates an approximation of the vesicularity of the magma: the lighter the color, the more vesicular.

'primitive', less dense, and less viscous than the degassed magma that descends from shallow levels in the plumbing system (Figure 1). Convective magma transport driven by density difference may also occur below shallow magma chambers.

[7] At shallow levels in the plumbing system the ascent of volatiles is achieved mainly in the form of bubbles, producing a two-phase flow (Figure 1); the depth at which this occurs is specific to each system as it depends on the total volatile budget and solubility relationships of the magma. Once the bubbles are sufficiently large, the gas phase may segregate from the melt. The increased ascent speed relative to melt, and possibly coalescence may lead to slug flow and/or enhancement of turbulence in the melt phase. Near the surface the magma density increases owing to the loss of the gas phase, crystallization, and overall cooling. The changes in properties of this magma, particularly its density and viscosity, constrain the rate of convection. A transitional zone exists at depths at which the bubble size increases to the point where the relative velocity of individual bubbles to that of the melt is no longer negligible. Above this zone, the magma properties change considerably owing to the exsolution of water. Below this level it is likely that most of the gas phase is $CO_2$. In the model presented here the transitional and shallow-level two-phase flow zones are not considered, so that the development and characteristics of convection and outgassing determined are those associated with the lower conduit plumbing where the role of the segregated gas phase can be neglected. Assuming that the level of the magma free-surface remains constant, and assuming that there is no net effusion of magma, conservation of mass dictates that the average rate of ascent and descent of magma, above and below the transitional zone, also remains constant. Both assumptions are reasonable and consistent with observations at persistently degassing volcanoes such as Villarrica and Erebus [*Palma et al.*, 2008; *Oppenheimer et al.*, 2009]. Here we assert therefore, that the rate of convection below the transitional zone (as modeled in this paper) constrains the rate of magma degassing at the surface.

## 2.2. Convective Flux in Narrow Conduits

### 2.2.1. Dimensional Analysis

[8] Magma convection is modeled here assuming that magma flows as an incompressible fluid inside a vertical or tilted cylinder or slot. The flux of gas and

heat through the conduit wall are considered negligible. Variables such as temperature and crystallization rate are not incorporated directly in this analysis, although temperature variations are implicitly considered as one source of changes in density and viscosity of the melt. The models of *Kazahaya et al.* [1994] and *Stevenson and Blake* [1998] assumed that the fresh volatile-rich magma ascended in the core of the pipe and that degassed and more dense magma descended in the annulus (i.e. core-annular flow). Conservation of mass and volume dictates that the volumetric flow rate of both fluids must be equal within the conduit, as assumed in an open magmatic system where the degassed and more dense magma sinks and is replaced by the same volume of fresh magma from deeper levels. In this case, it is also assumed that the height of the magma column stays approximately at a static level.

[9] For the dimensional analysis of steady countercurrent flow, six variables describe the situation: the dynamic viscosities of the lighter (ascending) and heavier (descending) fluids $\mu_a$ and $\mu_d$, respectively; volumetric flow rate $Q$; the density of the descending fluid $\rho_d$; the reduced gravity $g' = g \cos\theta \, \Delta\rho/\rho_d$, where $\theta$ is the angle of inclination of the pipe, $g$ is the value of gravity, $\Delta\rho$ is the density difference between the fluids; and the characteristic length-scale of the conduit $R$, which is the radius of the cylindrical pipe. These six variables involve three primary dimensions (mass, length and time) so that the system can be described by three dimensionless groups. The first dimensionless group is the viscosity ratio:

$$\kappa = \frac{\mu_a}{\mu_d} \tag{1}$$

The second dimensionless group is the Grashof number:

$$Gr = \frac{g'R^3}{\nu_d^2} \tag{2}$$

where $\nu_d$ is the kinematic viscosity of the descending fluid ($\mu_d/\rho_d$). The Grashof number compares viscous to buoyancy forces and it can indicate the transition between flow regimes in boundary layers and buoyancy-driven flows [e.g., *Jaluria*, 2003; *Jin and Chen*, 1996; *Bratsun et al.*, 2003]. Note that these two groups depend on the properties of the fluids and geometry of the conduit only. The third dimensionless group is the Reynolds number, which

incorporates inertial forces by considering the volumetric flow rate, $Q$:

$$Re = \frac{Q}{\nu_d R} \tag{3}$$

Here the Reynolds number is effectively an expression for the volumetric flow rate in dimensionless form. Note that in the definition of $Gr$ and $Re$ the viscous dissipation is controlled by the descending fluid. Regarding the selection of a characteristic length, no restrictions have been imposed on the geometry or inclination of the conduit.

### 2.2.2. Core-Annular Flow

[10] The equations and dynamics of core-annular flow in vertical pipes have been analyzed previously by *Hickox* [1971], *Arney et al.* [1993] and *Huppert and Hallworth* [2007]. In this work the theory is expanded to consider the flow in a slot (or dike) (see Appendix A). This analysis of the flow rate during countercurrent flow of two immiscible fluids in a conduit governed by the balance between buoyancy and viscous forces, where the buoyancy force depends on the density difference between the two fluids, yields another dimensionless group: the flux coefficient,

$$C_Q = \frac{Q\nu_d}{g'R^4} = \frac{Re}{Gr} \tag{4}$$

The flux coefficient represents the ratio of viscous and inertial forces to buoyancy forces, and is related to the solution of the countercurrent perfect core–annular flow (equation (A10)). *Huppert and Hallworth* [2007] used this dimensionless group to parameterize their laboratory results in vertical pipes. For the case of core-annular flow in vertical pipes the flux coefficient determines the relationship between the pressure drop and position of the interface for a given viscosity ratio (Appendix A). Here, $C_Q$ equals the normalized volumetric flux of the ascending and descending fluids (see equations (A10)–(A12)). Note that $Q$ can be expressed by the product of the flow cross-sectional area and the averaged flow velocity, giving the relationship between the flux coefficient and the Poiseuille number, $Po$, used by *Stevenson and Blake* [1998],

$$C_Q = \frac{Q\mu_d}{g\Delta\rho R^4} = \pi\alpha^2 Po \tag{5}$$

where $\alpha$ is the fraction of the radius occupied by the fluid in the core of the flow. Using equation (5) the
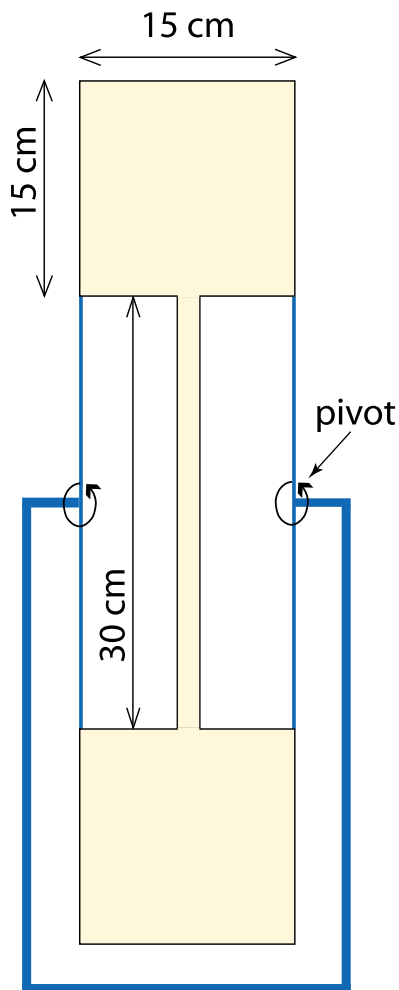
**Figure 2.** Sketch of the apparatus used in the two-tank experiments. Two 3.375-liter tanks are connected by a cylindrical pipe and attached to a metal structure that allows the inclination of the apparatus.

values of $Q$ and $C_Q$ are calculated from the results of *Stevenson and Blake* [1998] setting $\alpha$ to 0.6 for those experiments where this value was not specified.

[11] Therefore, the volumetric flux of the ascending fluid in a conduit arranged at any angle is:

$$Q = Re\, \nu_d R = C_Q \frac{g' R^4}{\nu_d}. \qquad (6)$$

## 2.3. Equivalent Radius

[12] The flow rate of the two-fluid convection is strongly dependent on the radius of the pipe (equation (6)). Previous investigations on the degassing rate at open vent volcanoes have used this relationship to estimate the radius of the conduit

[e.g., *Witter et al.*, 2004; *Stix*, 2007]. However, the geometry of the plumbing system can be much more complex than a cylindrical pipe. Indeed, the conduit might alternatively consist of a dike or more than one pipe (e.g., Stromboli volcano [*Ripepe et al.*, 2005; *Mattia et al.*, 2004]). The relationship between the volume flux of magma in a cylindrical pipe, a dike, or a branch of pipes can be shown to be linear (see Appendix A). For example, if a flow rate $Q$ is obtained with a pipe of radius $R$, doubling the flow rate can be achieved with two pipes of the same radius, or by increasing the radius of the pipe by a factor of 1.19. The relationship between the volume flow rate and properties of the magma in the case of countercurrent flow in a slot is identical to that of countercurrent flow in pipes (Appendix A2). Therefore, the same flow rate $Q$ can be obtained in a dike whose width can be related to the radius of the pipe.

[13] Consequently, we suggest here that the radius of the conduit calculated with the convection model is better considered as an *equivalent radius*. The equivalent radius is the radius of a cylindrical pipe in which buoyancy-driven convection reaches the same flow rate calculated for a real system of unknown geometry. Thus, the equivalent radius does not necessarily represent the actual geometry of the conduit but it yields an estimate of its dimensions, and can be used in any plumbing system regardless of its geometry. Note, henceforth we use the term 'conduit' to refer to any pathway for magma without any geometric connotations.

## 3. Laboratory Experiments

### 3.1. Experimental Design

[14] Laboratory experiments were conducted in order to study the convection of two fluids in a pipe that occurs owing to their density difference as a function of the dimensionless parameters identified in the previous section, allowing comparison with natural volcanic systems.

[15] The experimental apparatus consisted of two cubic perspex tanks, $3.375 \cdot 10^{-3}$ m$^3$ each, connected by a 30 cm long circular pipe (Figure 2). The apparatus was attached to a metal frame and was able to rotate freely (360°) about a pivot located at the center point between the tanks, so that the axis of rotation was perpendicular to the pipe. Most experiments were conducted using a 10 mm radius pipe, but two experiments were performed with a pipe of 25 mm radius.

[16] Most of the experiments involved immiscible fluids. A few experiments were conducted using miscible fluids with the aim of comparing the flow characteristics to those observed for immiscible fluids. The fluids chosen for the experiments were organic oils and variable mixtures of glycerol or golden syrup with water. We used vegetable, corn and sunflower oils with densities and viscosities within the ranges 897–921 kg m$^{-3}$ and 0.07–0.2 Pa s, respectively. While pure water has a density of 1000 kg m$^{-3}$ and a viscosity of 0.001 Pa s, the water-diluted glycerol and golden syrup have a density and viscosity of up to 1419 kg m$^{-3}$ and 5.3 Pa s (pure golden syrup), respectively.

[17] The experiments were photographed and video recorded to facilitate a later inspection of the flow characteristics. On some occasions, blue, red or green dye was added to one of the fluids to provide better visualization of the flow. Initially, the interface between the fluids could be in the bottom or upper tank near the junction with the pipe, or near the middle of the pipe. Once the apparatus had been filled with the two chosen fluids, the experiment was started by creating an unstable fluid stratification by simply rotating the apparatus through 180°.

[18] The volume flux of the convecting fluids was calculated by measuring the position of the horizontal interface in the tanks as a function of time. The volume flux of the fluids moving from one tank to the other through the pipe was found to be constant throughout an experiment, with the readings showing very high precision as evidenced by a high correlation factor. A summary of the experiments that includes the properties of the fluids and volumetric fluxes is presented in Tables 1 and 2.

## 3.2. Characteristics of the Flow

[19] Several arrangements of fluid flow were observed in these experiments, particularly with the pipe in a vertical or near–vertical position. Variations in the arrangement of the flow in pipes are quite typical of immiscible fluid-fluid flows [*Joseph and Renardy*, 1993a]. Among the most common arrangements, our experiments of countercurrent flow showed (1) wavy core–annular flow, (2) medium-sized to large blobs (relative to the radius of the pipe) of the lighter fluid rising through the continuous denser fluid, (3) small to medium-sized blobs of the heavier fluid sinking through continuous lighter fluid, (4) thin and non–uniform threads of the heavier fluid, and (5) stratified flow with the lighter

fluid on top of the heavier fluid. Detailed investigation of these flow patterns is beyond the scope of this paper. Here we concentrate on how the flow characteristics influenced the variation in the volumetric flow rate of the fluids. Nevertheless, it is noteworthy that the 'perfect' core–annular flow configuration was found only under very specific circumstances, and this has important implications for the widespread application of the core–annular concept to natural volcanic systems. The conditions for countercurrent core–annular flow and the consequences of the development of different flow patterns are discussed below.

### 3.2.1. Vertical Pipe

[20] The experiments performed with the apparatus in a vertical position were characterized by different fluid arrangements and flow patterns (Figure 3): (1) unsteady core-annular flow (UCA), (2) pseudo–stratified flow (PS), and (3) blobs or turbulent flow (BT). The volumetric flow rate remained constant throughout individual experiments despite the variable flow pattern shown by some experiments.

[21] In the first category (UCA), the core–annular flow generally had wavy vertical interfaces. These waves commonly propagated along the pipe and, after a few seconds, provoked the breakdown of the core-annular configuration. Long blobs, which are also considered here as part of UCA flow, also experienced waves at the interface (Figure 3a). Two distinct but similar flow patterns were termed pseudo–stratified (PS) flow: fluids flowing on opposite sides of the pipe, and thin threads of the heavier fluid descending next to the wall (Figure 3b). The first arrangement was common in experiments with oil and both pure and diluted glycerol (Table 1, experiments 524b, 801a, 801b). In this pseudo-stratification the position of the interface, as well as the thickness of the streams, changed with time and with the position along the pipe. The development of a thin thread descending on one side of the pipe was characteristic of golden syrup in oil (Table 1).

[22] Two experiments with diluted golden syrup and oil showed big blobs (size comparable to the diameter of the pipe; Table 1, exp. 807a, 808b) and small-sized blobs of syrup dispersed in the continuous oil (Figure 3c). The blobs of syrup descended through the middle of the pipe and oscillated from one side of the pipe to the other. On some occasions, these blobs could amalgamate and form a more continuous but irregular stream of syrup. The small blobs could either descend on one side of the pipe or some of

**Table 1.** Summary of the Experimental Data and Results for Experiments in Vertical Pipes[a]

| Experiment | Fluid | | Density | | Kinematic Viscosity | | Pipe, R (mm) | Volume Flux (m³/s) | Pattern | | | IPI[b] | $\kappa$ | $C_Q$ |
| | Light | Heavy | $\rho_l$ (kg/m³) | $\rho_h$ (kg/m³) | $\nu_l$ (m²/s) | $\nu_h$ (m²/s) | | | Pipe | Top Tank | Bottom Tank | | | |
|---|---|---|---|---|---|---|---|---|---|---|---|---|---|---|
| 816a | water | gly p | 1000.0 | 1253.8 | $1.085\cdot10^{-6}$ | $1.584\cdot10^{-3}$ | 10 | $1.289\cdot10^{-6}$ | UCA, BT | LSN | TP | T | $5.46\cdot10^{-4}$ | $1.03\cdot10^{-1}$ |
| 824a | oil-s | syr-p | 915.6 | 1418.8 | $1.928\cdot10^{-4}$ | $3.746\cdot10^{-2}$ | 10 | $1.187\cdot10^{-7}$ | PS | B | LS | B | $3.32\cdot10^{-3}$ | $1.28\cdot10^{-1}$ |
| 524a | oil-v | gly p | 917.3 | 1253.8 | $1.983\cdot10^{-4}$ | $1.584\cdot10^{-3}$ | 10 | $1.528\cdot10^{-6}$ | UCA | B, LSN | LS | P | $9.16\cdot10^{-2}$ | $9.20\cdot10^{-2}$ |
| 524b | oil-v | gly p | 917.3 | 1253.8 | $1.983\cdot10^{-4}$ | $1.584\cdot10^{-3}$ | 10 | $2.983\cdot10^{-6}$ | PS | LSN | LS | P | $9.16\cdot10^{-2}$ | $1.80\cdot10^{-1}$ |
| 525a | oil-v | gly p | 917.3 | 1253.8 | $1.983\cdot10^{-4}$ | $1.584\cdot10^{-3}$ | 10 | $2.690\cdot10^{-6}$ | UCA, PS | LSN | LS | P | $9.16\cdot10^{-2}$ | $1.62\cdot10^{-1}$ |
| 525b | oil-v | gly p | 917.3 | 1253.8 | $1.983\cdot10^{-4}$ | $1.584\cdot10^{-3}$ | 10 | $2.740\cdot10^{-6}$ | UCA, PS | LSN | LS | P | $9.16\cdot10^{-2}$ | $1.65\cdot10^{-1}$ |
| 521a | oil-c | gly p | 900.8 | 1260.5 | $2.252\cdot10^{-4}$ | $1.313\cdot10^{-3}$ | 25 | $6.176\cdot10^{-5}$ | BT | LS | | T | $1.23\cdot10^{-1}$ | $7.42\cdot10^{-2}$ |
| 522a | oil-c | gly p | 911.8 | 1256.9 | $2.252\cdot10^{-4}$ | $1.313\cdot10^{-3}$ | 25 | $6.559\cdot10^{-5}$ | BT | LS | | B | $1.24\cdot10^{-1}$ | $8.19\cdot10^{-2}$ |
| 801a | oil-v | gly d | 921.0 | 1236.5 | $1.924\cdot10^{-4}$ | $4.846\cdot10^{-4}$ | 10 | $5.929\cdot10^{-6}$ | PS | LSN | LS | B | $2.96\cdot10^{-1}$ | $1.15\cdot10^{-1}$ |
| 801c | oil-v | gly d | 921.0 | 1236.5 | $1.924\cdot10^{-4}$ | $4.846\cdot10^{-4}$ | 10 | $4.377\cdot10^{-6}$ | PS | LSN | LS | B | $2.96\cdot10^{-1}$ | $8.48\cdot10^{-2}$ |
| 807a | oil-v | syr-d | 921.0 | 1216.0 | $1.924\cdot10^{-4}$ | $2.151\cdot10^{-5}$ | 10 | $7.694\cdot10^{-6}$ | BT, PS | | LSB, LS | P | $6.77\cdot10^{0}$ | $6.96\cdot10^{-3}$ |
| 808a | oil-v | syr-d | 921.0 | 1216.0 | $1.924\cdot10^{-4}$ | $2.151\cdot10^{-5}$ | 10 | $6.595\cdot10^{-6}$ | BT, PS | | LS | P | $6.77\cdot10^{0}$ | $5.97\cdot10^{-3}$ |
| 808b | oil-v | syr-d | 921.0 | 1216.0 | $1.924\cdot10^{-4}$ | $2.151\cdot10^{-5}$ | 10 | $7.899\cdot10^{-6}$ | BT, PS | | LS | P | $6.77\cdot10^{0}$ | $7.14\cdot10^{-3}$ |
| 808c | oil-v | syr-d | 921.0 | 1216.0 | $1.924\cdot10^{-4}$ | $2.151\cdot10^{-5}$ | 10 | $7.988\cdot10^{-6}$ | BT, PS | | LS | P | $6.77\cdot10^{0}$ | $7.23\cdot10^{-3}$ |
| 809a | oil-v | gly d | 917.3 | 1104.5 | $1.983\cdot10^{-4}$ | $1.234\cdot10^{-5}$ | 10 | $6.573\cdot10^{-6}$ | BT, PS | LSB | LSB, LS | T | $1.33\cdot10^{1}$ | $4.88\cdot10^{-3}$ |
| 809b | oil-v | gly d | 917.3 | 1104.5 | $1.983\cdot10^{-4}$ | $1.234\cdot10^{-5}$ | 10 | $4.988\cdot10^{-6}$ | BT, PS | LSB, LS | LSB, LS | T | $1.33\cdot10^{1}$ | $3.71\cdot10^{-3}$ |
| 809c | oil-v | gly d | 917.3 | 1104.5 | $1.983\cdot10^{-4}$ | $1.234\cdot10^{-5}$ | 10 | $3.533\cdot10^{-6}$ | BT, PS | LSB, LS | LSB, LS | T | $1.33\cdot10^{1}$ | $2.63\cdot10^{-3}$ |
| 814a | oil-v | gly d | 917.3 | 1104.5 | $1.983\cdot10^{-4}$ | $1.234\cdot10^{-5}$ | 10 | $5.619\cdot10^{-6}$ | BT | LSN | LS | T | $1.33\cdot10^{1}$ | $4.18\cdot10^{-3}$ |
| 426a | oil-c | water | 897.1 | 1000.0 | $2.252\cdot10^{-4}$ | $1.085\cdot10^{-6}$ | 10 | $2.061\cdot10^{-6}$ | UCA, PS | LSB | LSB | P | $1.86\cdot10^{2}$ | $2.22\cdot10^{-4}$ |
| 426b | oil-c | water | 897.1 | 1000.0 | $2.252\cdot10^{-4}$ | $1.085\cdot10^{-6}$ | 10 | $1.774\cdot10^{-6}$ | UCA | LSB | LSB | P | $1.86\cdot10^{2}$ | $1.91\cdot10^{-4}$ |

[a]Fluid abbreviations: oil-s, oil-v and oil-c correspond to sunflower, vegetable and corn oil, respectively; gly p and gly d correspond to glycerol pure and diluted, respectively; syr-d is diluted golden syrup. Pattern abbreviation: in the pipe UCA = unsteady core–annular flow, BT = blobs or turbulent flow, PS = pseudo-stratified flow; in the tanks B = blobs, LSB = laminaar stream and blobs, LSN = laminar stream with non-uniform thickness, LS = laminar stream, TP = turbulent plume.

[b]Initial position of the interface before flipping the apparatus up-side down: P = near the middle of the pipe, T = in the top tank, B = in the bottom tank.

**Table 2.** Summary of the Experimental Data and Results for Experiments With Inclined Pipes[a]

| Experiment | Fluid | | Density | | Kinematic Viscosity | | Pipe, R (mm) | Pipe, ang (deg) | Volume Flux (m³/s) | Pattern | | | IPI[b] | $\kappa$ | $C_Q$ |
| | Light | Heavy | $\rho_l$ (kg/m³) | $\rho_h$ (kg/m³) | $\nu_l$ (m²/s) | $\nu_{l_h}$ (m²/s) | | | | Pipe | Top Tank | Bottom Tank | | | |
| --- | --- | --- | --- | --- | --- | --- | --- | --- | --- | --- | --- | --- | --- | --- | --- |
| 731c | air | gly d | 1.22 | 1236.5 | $1.475 \cdot 10^{-5}$ | $4.846 \cdot 10^{-4}$ | 10 | 6 | $3.630 \cdot 10^{-5}$ | ST | | | B | $3.00 \cdot 10^{-5}$ | $1.81 \cdot 10^{-1}$ |
| 731a | air | gly d | 1.22 | 1236.5 | $1.475 \cdot 10^{-5}$ | $4.846 \cdot 10^{-4}$ | 10 | 11 | $3.768 \cdot 10^{-5}$ | ST | | | B | $3.00 \cdot 10^{-5}$ | $1.90 \cdot 10^{-1}$ |
| 731b | air | gly d | 1.22 | 1236.5 | $1.475 \cdot 10^{-5}$ | $4.846 \cdot 10^{-4}$ | 10 | 23 | $4.162 \cdot 10^{-5}$ | ST | | | B | $3.00 \cdot 10^{-5}$ | $2.24 \cdot 10^{-1}$ |
| 727a | water | gly p | 1000.0 | 1261.5 | $1.085 \cdot 10^{-3}$ | $1.501 \cdot 10^{-3}$ | 10 | 16 | $3.962 \cdot 10^{-6}$ | ST | LSN | LS | B | $5.73 \cdot 10^{-4}$ | $3.05 \cdot 10^{-1}$ |
| 911a | oil-s | syr-p | 915.6 | 1418.8 | $1.928 \cdot 10^{-4}$ | $3.746 \cdot 10^{-2}$ | 10 | 7 | $2.450 \cdot 10^{-7}$ | ST | B | LS | B | $3.32 \cdot 10^{-3}$ | $2.66 \cdot 10^{-1}$ |
| 911a2 | oil-s | syr-p | 915.6 | 1418.8 | $1.928 \cdot 10^{-4}$ | $3.746 \cdot 10^{-2}$ | 10 | 7 | $1.989 \cdot 10^{-7}$ | STI | B | LS | B | $3.32 \cdot 10^{-3}$ | $2.16 \cdot 10^{-1}$ |
| 823a | oil-s | syr-p | 915.6 | 1418.8 | $1.928 \cdot 10^{-4}$ | $3.746 \cdot 10^{-2}$ | 10 | 15 | $1.798 \cdot 10^{-7}$ | ST | LS | LS | B | $3.32 \cdot 10^{-3}$ | $2.01 \cdot 10^{-1}$ |
| 1203a | oil-s | syr-p | 915.6 | 1418.8 | $1.928 \cdot 10^{-4}$ | $3.746 \cdot 10^{-2}$ | 10 | 31 | $2.280 \cdot 10^{-7}$ | ST | | LS | B | $3.32 \cdot 10^{-3}$ | $2.87 \cdot 10^{-1}$ |
| 524c | oil-v | gly p | 917.3 | 1261.5 | $1.983 \cdot 10^{-4}$ | $1.584 \cdot 10^{-3}$ | 10 | 6 | $2.906 \cdot 10^{-6}$ | ST | LS | LS | P | $9.10 \cdot 10^{-2}$ | $1.73 \cdot 10^{-1}$ |
| 622c | oil-v | gly p | 917.3 | 1261.5 | $1.983 \cdot 10^{-4}$ | $1.584 \cdot 10^{-3}$ | 10 | 12 | $2.524 \cdot 10^{-6}$ | ST | LSN | LS | P | $9.10 \cdot 10^{-2}$ | $1.53 \cdot 10^{-1}$ |
| 524d | oil-v | gly p | 917.3 | 1261.5 | $1.983 \cdot 10^{-4}$ | $1.584 \cdot 10^{-3}$ | 10 | 23 | $3.130 \cdot 10^{-6}$ | ST | LS | LS | P | $9.10 \cdot 10^{-2}$ | $2.01 \cdot 10^{-1}$ |
| 622a | oil-v | gly p | 917.3 | 1261.5 | $1.983 \cdot 10^{-4}$ | $1.584 \cdot 10^{-3}$ | 10 | 24 | $2.269 \cdot 10^{-6}$ | ST | LSN | LS | P | $9.10 \cdot 10^{-2}$ | $1.47 \cdot 10^{-1}$ |
| 622b | oil-v | gly p | 917.3 | 1261.5 | $1.983 \cdot 10^{-4}$ | $1.584 \cdot 10^{-3}$ | 10 | 36 | $2.230 \cdot 10^{-6}$ | ST | LSN | LS | P | $9.10 \cdot 10^{-2}$ | $1.63 \cdot 10^{-1}$ |
| 524e | oil-v | gly p | 917.3 | 1261.5 | $1.983 \cdot 10^{-4}$ | $1.584 \cdot 10^{-3}$ | 10 | 40 | $2.709 \cdot 10^{-6}$ | ST | LS | LS | P | $9.10 \cdot 10^{-2}$ | $2.09 \cdot 10^{-1}$ |
| 801d | oil-v | gly d | 921.0 | 1236.5 | $1.924 \cdot 10^{-4}$ | $4.846 \cdot 10^{-4}$ | 10 | 9 | $6.487 \cdot 10^{-6}$ | ST | LS | LS | B | $2.96 \cdot 10^{-1}$ | $1.27 \cdot 10^{-1}$ |
| 801b | oil-v | gly d | 921.0 | 1236.5 | $1.924 \cdot 10^{-4}$ | $4.846 \cdot 10^{-4}$ | 10 | 18 | $7.054 \cdot 10^{-6}$ | ST | LS | LS | B | $2.96 \cdot 10^{-1}$ | $1.44 \cdot 10^{-1}$ |
| 808g | oil-v | syr-d | 921.0 | 1216.0 | $1.924 \cdot 10^{-4}$ | $2.151 \cdot 10^{-5}$ | 10 | 4 | $6.459 \cdot 10^{-6}$ | STI | | LS | P | $6.77 \cdot 10^{0}$ | $5.86 \cdot 10^{-3}$ |
| 808h | oil-v | syr-d | 921.0 | 1216.0 | $1.924 \cdot 10^{-4}$ | $2.151 \cdot 10^{-5}$ | 10 | 9 | $7.342 \cdot 10^{-6}$ | STI | | LS | P | $6.77 \cdot 10^{0}$ | $6.72 \cdot 10^{-3}$ |
| 808d | oil-v | syr-d | 921.0 | 1216.0 | $1.924 \cdot 10^{-4}$ | $2.151 \cdot 10^{-5}$ | 10 | 12 | $9.625 \cdot 10^{-6}$ | ST | | LS | P | $6.77 \cdot 10^{0}$ | $8.90 \cdot 10^{-3}$ |
| 807b | oil-v | syr-d | 921.0 | 1216.0 | $1.924 \cdot 10^{-4}$ | $2.151 \cdot 10^{-5}$ | 10 | 20 | $1.146 \cdot 10^{-5}$ | ST | LS | LS | P | $6.77 \cdot 10^{0}$ | $1.10 \cdot 10^{-2}$ |
| 808f | oil-v | syr-d | 921.0 | 1216.0 | $1.924 \cdot 10^{-4}$ | $2.151 \cdot 10^{-5}$ | 10 | 24 | $1.058 \cdot 10^{-5}$ | ST | | LS | P | $6.77 \cdot 10^{0}$ | $1.05 \cdot 10^{-2}$ |
| 808e | oil-v | syr-d | 921.0 | 1216.0 | $1.924 \cdot 10^{-4}$ | $2.151 \cdot 10^{-5}$ | 10 | 28 | $1.160 \cdot 10^{-5}$ | ST | | LS | P | $6.77 \cdot 10^{0}$ | $1.19 \cdot 10^{-2}$ |
| 814c | oil-v | gly d | 917.3 | 1104.5 | $1.983 \cdot 10^{-4}$ | $1.234 \cdot 10^{-5}$ | 10 | 6 | $5.032 \cdot 10^{-6}$ | STI | | | T | $1.33 \cdot 10^{1}$ | $3.76 \cdot 10^{-4}$ |
| 814b | oil-v | gly d | 917.3 | 1104.5 | $1.983 \cdot 10^{-4}$ | $1.234 \cdot 10^{-5}$ | 10 | 16 | $6.841 \cdot 10^{-6}$ | ST | | | T | $1.33 \cdot 10^{1}$ | $5.29 \cdot 10^{-3}$ |
| 814d | oil-v | gly d | 917.3 | 1104.5 | $1.983 \cdot 10^{-4}$ | $1.234 \cdot 10^{-5}$ | 10 | 31 | $7.707 \cdot 10^{-6}$ | ST | | | T | $1.33 \cdot 10^{1}$ | $6.68 \cdot 10^{-3}$ |
| 427c | oil-c | water | 897.1 | 1000.0 | $2.252 \cdot 10^{-4}$ | $1.085 \cdot 10^{-6}$ | 10 | 6 | $6.106 \cdot 10^{-6}$ | ST | LS | LS | P | $1.86 \cdot 10^{2}$ | $6.60 \cdot 10^{-4}$ |
| 427c2 | oil-c | water | 897.1 | 1000.0 | $2.252 \cdot 10^{-4}$ | $1.085 \cdot 10^{-6}$ | 10 | 6 | $2.572 \cdot 10^{-6}$ | STI | LS | LS | P | $1.86 \cdot 10^{2}$ | $2.78 \cdot 10^{-4}$ |
| 428a | oil-c | water | 897.1 | 1000.0 | $2.252 \cdot 10^{-4}$ | $1.085 \cdot 10^{-6}$ | 10 | 15 | $6.645 \cdot 10^{-6}$ | ST,STI | B | LS | P | $1.86 \cdot 10^{2}$ | $7.40 \cdot 10^{-4}$ |
| 427a | oil-c | water | 897.1 | 1000.0 | $2.252 \cdot 10^{-4}$ | $1.085 \cdot 10^{-6}$ | 10 | 21 | $6.514 \cdot 10^{-6}$ | ST | | LS | P | $1.86 \cdot 10^{2}$ | $7.50 \cdot 10^{-4}$ |
| 428b | oil-c | water | 897.1 | 1000.0 | $2.252 \cdot 10^{-4}$ | $1.085 \cdot 10^{-6}$ | 10 | 35 | $6.474 \cdot 10^{-6}$ | ST | | LS | P | $1.86 \cdot 10^{2}$ | $8.50 \cdot 10^{-4}$ |
| 427b | oil-c | water | 897.1 | 1000.0 | $2.252 \cdot 10^{-4}$ | $1.085 \cdot 10^{-6}$ | 10 | 50 | $6.035 \cdot 10^{-6}$ | ST | | LS | P | $1.86 \cdot 10^{2}$ | $1.01 \cdot 10^{-3}$ |

[a]Fluid abbreviations: oil-s, oil-v and oil-c correspond to sunflower, vegetable and corn oil, respectively; gly p and gly d correspond to glycerol pure and diluted, respectively; syr-d is diluted golden syrup. Pattern abbreviation: in thepipe ST = stratified flow, STI = stratified flow with instabilities; in the tanks B = blobs, LSB = laminar stream and blobs, LSN = laminar stream with non-uniform thickness, LS = laminar stream.

[b]Initial position of the interface before flipping the apparatus up–side down: P = near the middle of the pipe, T = in the top tank, B = in the bottom tank.
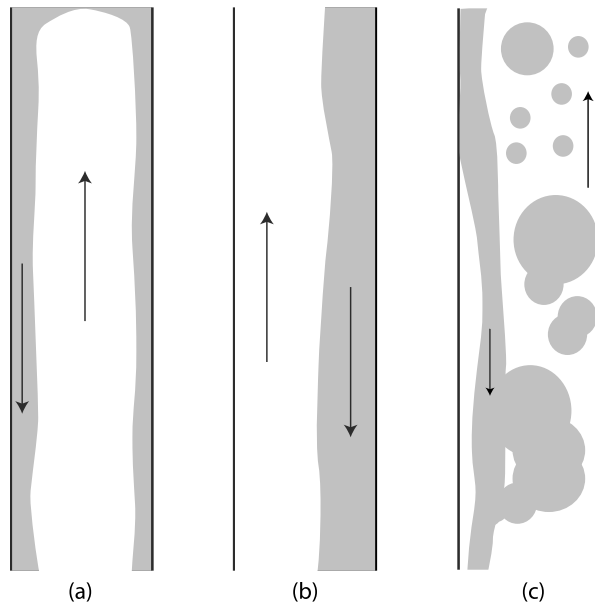
**Figure 3.** Illustrations of the flow patterns observed in vertical pipes. (a) Very long blobs with wavy interface as unsteady core–annular flow, (b) fluids flowing on opposite sides of the pipe as pseudo–stratified flow, and (c) blobs in a slightly turbulent flow. The dark region corresponds to the heavier fluid.

them rose, being pulled up by the ascending flow of oil. A similar pattern occurred with another experiment that involved oil and glycerol (Table 1, exp. 809c). Two experiments performed with the wider pipe of 25 mm radius exhibited turbulent flow (Table 1, exp. 521a, 522a), as seen in single-fluid flows at high Reynolds numbers.

### 3.2.2. Inclined Pipe

[23] With inclined pipes the flows were observed to be more stable than the flows in vertical pipes. Stratified flow (ST), with the lighter fluid flowing on top of the heavier one, dominated the countercurrent flow pattern at inclinations higher than 15 degrees (angle with respect to the vertical) (Figure 4a and Table 2). At lower inclinations, however, instabilities similar to those seen in vertical pipes were also observed, particularly at angles lower than 10 degrees (Figure 4b). For instance, with the pipe inclined at 6 degrees, the flow of oil and water exhibited water blobs or wavy vertical fluid interfaces (Table 2, exp. 427c2), and in experiments with golden syrup and oil the stream of syrup was not uniform in thickness along the pipe (Table 2).

[24] Despite the difficulty of observing the flow through the cylindrical pipe, some interesting observations of the interface between the fluids

could be made. The shape of the interface in stratified flow was found to be planar in most of the experiments, but curved in experiments that involved pure golden syrup. In some experiments with golden syrup and oil (824a in Table 1 and 911a2 in Table 2), the interface showed long wavelength undulations in the direction of the flow. Apparently, these waves originated at the upper pipe–tank junction and were related to the entrance of blobs of oil into the tank, which created oscillations in the cross-sectional area of both fluids. These oscillations would then propagate downstream without growing into major instabilities.

### 3.2.3. Miscible Fluids

[25] The flow of fluids with high viscosity contrast, using water and pure glycerol (viscosity ratio, $\kappa = 5.7 \cdot 10^{-4}$), exhibited slow mixing rates, evidenced by a constant flow rate of a laminar stratified flow at an inclination of 16 degrees, and by the clear identification of blobs and threads of glycerol in vertical pipes. In the case of the vertical pipe, most of the mixing occurred within the bottom tank, where the glycerol descended as a turbulent plume. With the pipe inclined, however, the glycerol sank through the bottom tank in a laminar manner. Using two miscible fluids with a low viscosity ratio (e.g., water with dilute glycerol or water with dilute golden syrup), mixing in the pipe was greater than in the
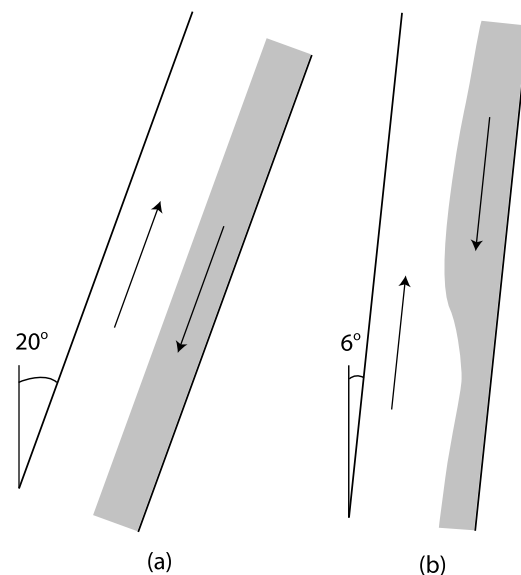


**Figure 4.** Illustrations of flow patterns observed in inclined pipes. (a) Well-defined steady stratified flow in a pipe inclined 20 degrees; (b) stratified flow with undulating interface in a pipe inclined at 6 degrees. The dark region corresponds to the heavier fluid.
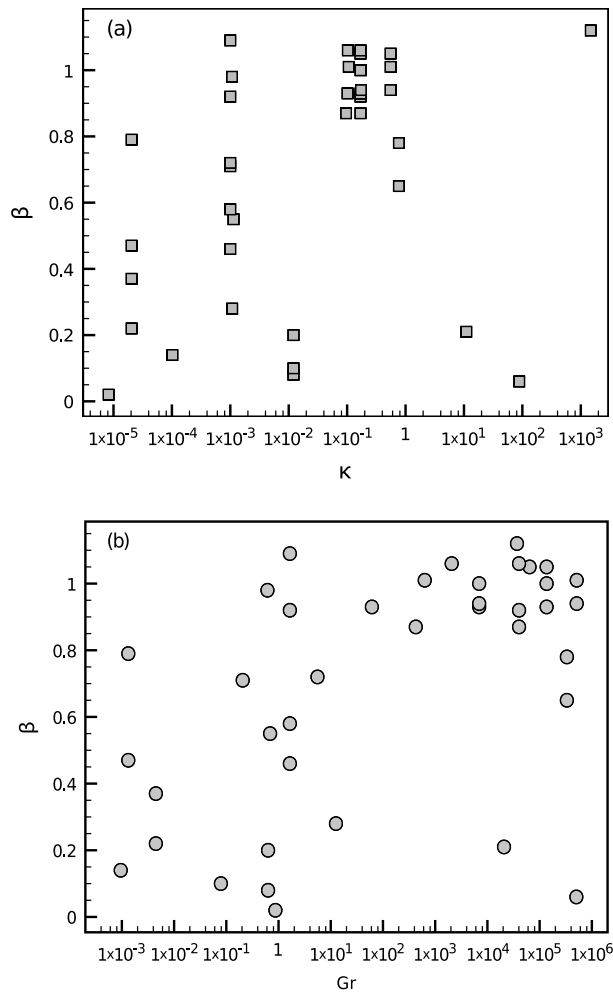
**Figure 5.** Plots of (a) the viscosity ratio and (b) the Grashof number with the extent of mixing ($\beta$) shown in experiments with miscible fluids. Data from *Huppert and Hallworth* [2007]. Note that for *Gr* > 100 most of the experiments exhibit high levels of mixing.

high viscosity contrast case. In this case, mixing within the tanks was so efficient that it was not possible to track the position of the interface, and so the volume flux could not be measured. These experiments were not included in the results presented in this paper.

[26] Similar observations were reported by *Huppert and Hallworth* [2007] from their experiments with miscible fluids in vertical pipes. They distinguished two flow patterns: vigorous turbulent mixing when both fluids had low viscosity, and core–annular flow with varicose instabilities with little or no mixing when there was a high viscosity contrast between the fluids. *Huppert and Hallworth* [2007] measured the extent of mixing through a parameter, $\beta$, where $\beta = 0$ implies no mixing and $\beta = 1$ represents complete mixing. Although these observations suggest that

the viscosity ratio may have a control on the mixing levels and flow regime of the countercurrent flow, the experimental results published by *Huppert and Hallworth* [2007] show that this cannot actually be the only controlling variable, as evidenced in Figure 5a. Rather, the extent of mixing seems to relate to the Grashof number (Figure 5b), although the *Gr* alone may not fully explain these variations.

## 3.3. Volume Flow Rate

[27] The experimental results reveal that the dimensionless flow rate (*Re*) is a function of *Gr*, with two regimes separated by a critical *Gr* of about 100 (Figure 6). For *Gr* < 100 the ratio between the Grashof and Reynolds numbers is constant, which implies a constant value of $C_Q$ (equation (4)). A good fit for all the data with *Gr* < 100 is obtained with $C_Q = 0.1$. However, experiments from *Stevenson and Blake* [1998] with the lowest *Gr* are best fit with $C_Q = 0.07$, whereas those with higher *Gr* are best fit with $C_Q = 0.03$. The upper bound, generally represented by experiments with inclined pipes, is obtained with $C_Q = 0.2$. It is noteworthy that experiments with both immiscible and miscible fluids fall within this trend, regardless of the extent of mixing or flow pattern during mixing.

[28] For large *Gr*, *Gr* > 100, the relationship between the Reynolds and Grashof numbers in experiments with little or no mixing is:

$$Re = 0.45 Gr^{\frac{1}{2}} \qquad (7)$$

where the multiplicative coefficient varies between 0.2 (lower bound) and 0.7 (upper bound). This equation can be re-arranged to show that it is equivalent to stating that the flow rate is given by a constant Froude number (*Fr*), where

$$Fr = C_Q Gr^{\frac{1}{2}} = \frac{Q}{g'^{\frac{1}{2}} R^{\frac{5}{2}}} \qquad (8)$$

Values of *Fr* for experiments with low or no mixing range from 0.2 to 0.8 and is independent of viscosity ratio (Figure 7). Several experiments that underwent strong mixing show a considerably lower flow rate (and thus lower *Re* and *Fr*).

[29] The values of the flux coefficient obtained in this work are in general agreement with those obtained by *Stevenson and Blake* [1998] and *Huppert and Hallworth* [2007] (Figure 8). Variations of $C_Q$ for a particular or similar pair of fluids (and similar viscosity ratio) are likely to be related to inaccuracies of the measurements, different flow patterns and miscibility of the fluids. Note that the
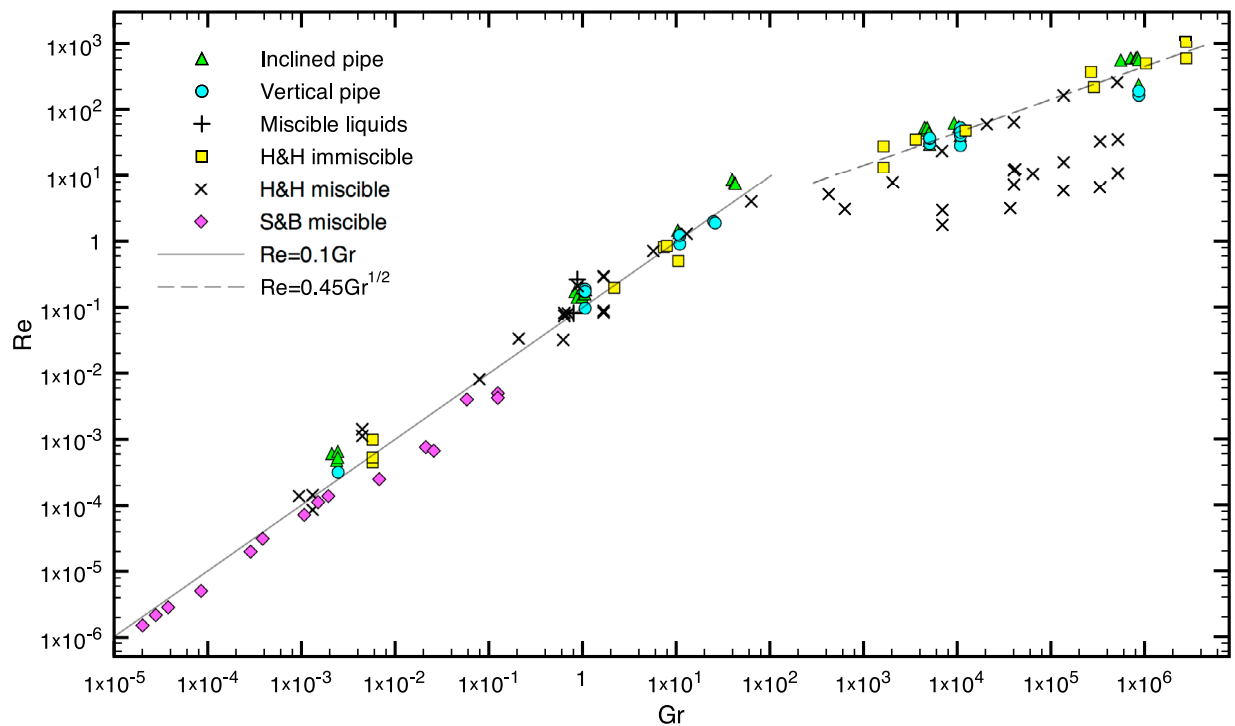
**Figure 6.** Relationship between the Reynolds number (dimensionless Q) and the Grashof number in experimental data. These data include our results as well as results from *Stevenson and Blake* [1998] (S&B) and *Huppert and Hallworth* [2007] (H&H). A good fit of the data for $Gr < 100$ is obtained with $C_Q = 0.1$. For $Gr > 100$ Re is related to the square root of Gr.

values of $C_Q$ obtained for inclined pipes are slightly higher than those obtained for vertical pipes (Figures 8 and 9). An explanation for this difference is the development of instabilities and flow patterns other than those that are core–annular. In effect, the experimental results presented here imply a relationship between the flow pattern and the steady volumetric flux. In general, experiments in vertical pipes carried out by *Stevenson and Blake* [1998] and some by *Huppert and Hallworth* [2007] that exhibited core–annular flow show the lowest values of $C_Q$ (Figure 8). Experiments that exhibited blobs or turbulent flow show slightly higher $C_Q$, and those that exhibited unsteady core-annular or pseudo–stratified flow can show even higher values of $C_Q$ (Figure 9). The values of $C_Q$ and $Fr$ slightly increase at higher inclination angles (Table 2). Experiments with the pipe inclined at the highest angles, which exhibited stratified flow, yielded the highest values of $C_Q$ (Figure 9). These results suggest that for any flow pattern developed within the pipe, the flux coefficient and Froude number lie in the range of values defined by the perfect core–annular flow (lower limit) and stratified flow (upper limit). This relationship may also be valid for the volumetric flux, although higher angles of inclination don't necessarily imply a higher Q.

[30] These results show that for vertical conduits and $Gr < 100$, $C_Q$ can be approximated as 0.1 whereas for inclined conduits $C_Q$ can be approximated as 0.2. This is the case for both immiscible and miscible fluids. Note that in volcanic systems the viscosity ratio between the ascending (volatile-rich) and descending (degassed) magmas is lower than unity, and most likely $\kappa < 0.1$, which further confirms the adequate choice for the value of $C_Q$. Indeed, high levels of mixing and a substantial decrease in the flux coefficient may be expected only at high Grashof numbers ($Gr > 100$). The utility of this approach is that the volumetric flow rate of the countercurrent flow of two fluids of known properties can be calculated using equation (6).

## 4. Application to Open-Vent Volcanoes

[31] Measurements of gas emissions yield valuable information about the characteristics of the magma and changes in the stability of the system [e.g., *Gerlach*, 1986; *Allard et al.*, 1994; *Shinohara and Witter*, 2005; *Allard et al.*, 2005; *Burton et al.*, 2007b]. Modeling magma degassing sustained by convection in conduits requires petrological information on melt composition, magmatic volatile
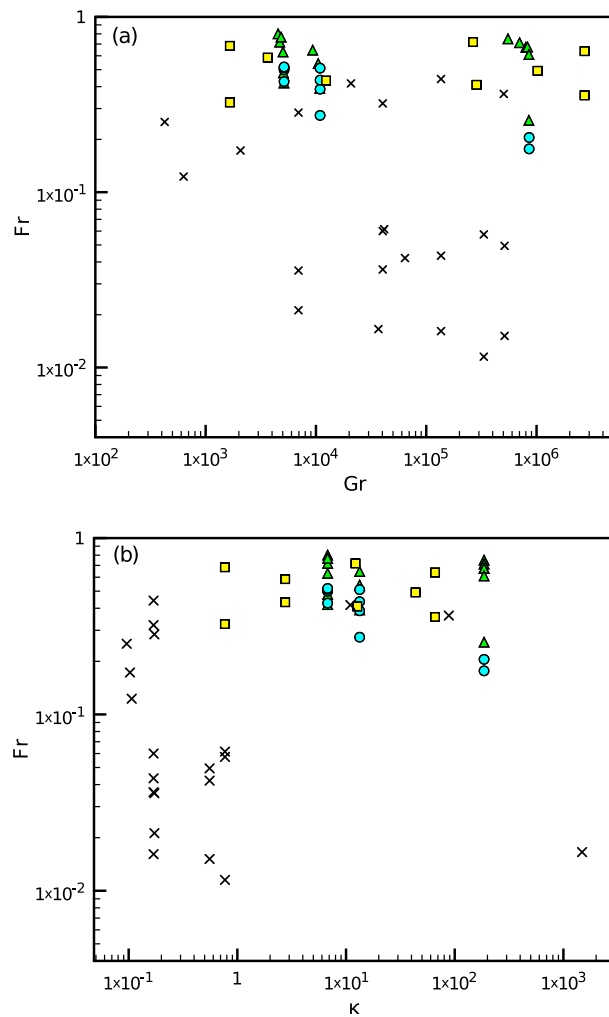
**Figure 7.** Plot of the Froude number versus (a) the Grashof number and (b) the viscosity ratio for experiments with Gr > 100. Symbols as in Figure 6.

content and crystal content for the calculation of the physical properties of both the source and degassed magma. Further, as discussed previously, the flow rate of magma ascent is also coupled with the dimensions of the conduit (equation (6)).

## 4.1. Physical Properties of Basaltic Magmas

[32] Quantification of magma flow in narrow conduits first requires calculation of the density and viscosity of both the volatile-rich and volatile-depleted magma. The density of the magma is given by:

$$\frac{1}{\rho_{l+cx}} = \frac{w_{cx}}{\rho_{cx}} + \frac{(1 - w_{cx})}{\rho_l} \qquad (9)$$

where $\rho_{l+cx}$ is the density of the mixture of crystals and melt, $\rho_{cx}$ and $\rho_l$ are the densities of the mineral

phase and melt, respectively, and $w_{cx}$ is the mass fraction of crystals. Estimates of the average density of olivine and plagioclase are 3500 and 2700 kg/m³, respectively. The equations of *Spera* [2000] were used to calculate the density of the melt, which takes into account the burden of dissolved water and carbon dioxide. Note that the vesicularity of the magma is not considered in the calculation of the mass fraction of crystals, $w_{cx}$.

[33] Melt viscosities were estimated with the parametric model of *Hui and Zhang* [2007]. This model estimates the viscosity of a wide range of melt compositions, from basalts to rhyolites, as well as their variations at different temperatures and water contents. *Giordano et al.* [2008] presented an alternative model based on the Vogel-Fulcher-Tammann (VFT) equation. Preference here was given to the *Hui and Zhang* [2007] model because based on a reanalysis of their data we believe their model performed slightly better at reproducing the data (even although that was actually contested by *Giordano et al.* [2008]). Moreover, most of the extra data used by *Giordano et al.* [2008] are associated with compositions other than the ones dealt with in this paper. The presence of crystals within the melt can increase the magma's viscosity 2 to 8 times for a volume fraction as low as 25%. This viscosity increase also depends on the shape and size distribution of the crystals, their maximum packing concentration and the non-Newtonian behavior at high concentrations [*McBirney and Murase*, 1984; *Pinkerton and Stevenson*, 1992; *Spera*, 2000; *Lavallée et al.*, 2007; *Costa et al.*, 2009]. Nevertheless, the most important factors governing the viscosity of magmas with low crystal contents, where the behavior can be approximated as Newtonian, are the viscosity of the liquid phase and the particle concentration [*Marsh*, 1981; *Pinkerton and Stevenson*, 1992]. In this case, the well known Einstein-Roscoe formula is a good approximation [e.g., *Pinkerton and Stevenson*, 1992; *Ishibashi and Sato*, 2007]:

$$\frac{\mu_{l+cx}}{\mu_l} = \left(1 - \frac{\varphi_{cx}}{\varphi_{max}}\right)^{-n} \qquad (10)$$

where $\mu_{l+cx}$ and $\mu_l$ are the viscosities of the magma (mixture melt plus crystals) and melt, respectively, $\varphi_{cx}$ the volume fraction of crystals, $n$ a parameter equal to 2.5, and $\varphi_{max}$ the maximum packing concentration (0.6). It is known that the viscosity of the mixture also has a strain rate dependency [e.g., *Gay et al.*, 1969; *McBirney and Murase*, 1984; *Ishibashi*, 2009; *Costa et al.*, 2009]. For instance, *Gay et al.* [1969] developed equations for the viscosity of the
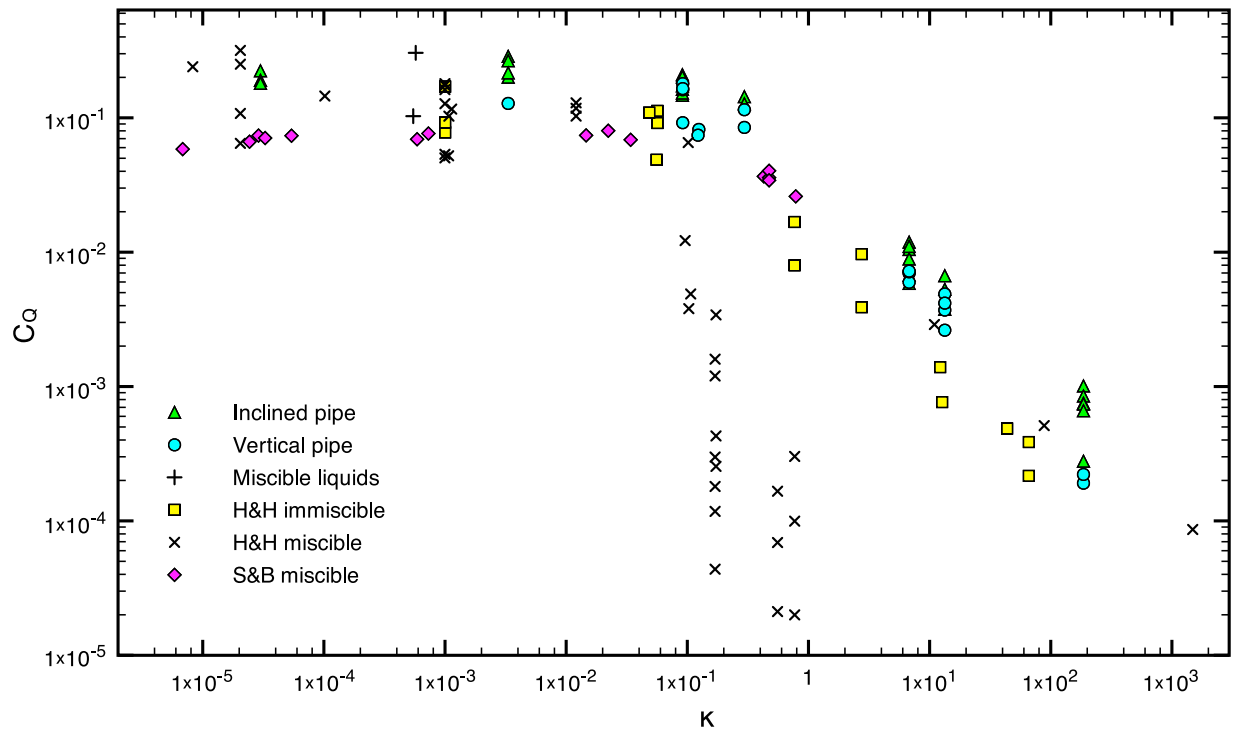
**Figure 8.** Flux coefficient calculated from experiments with vertical and inclined pipes for a wide range of viscosity ratios. These data include our results as well as results from *Stevenson and Blake* [1998] (S&B) and *Huppert and Hallworth* [2007] (H&H).
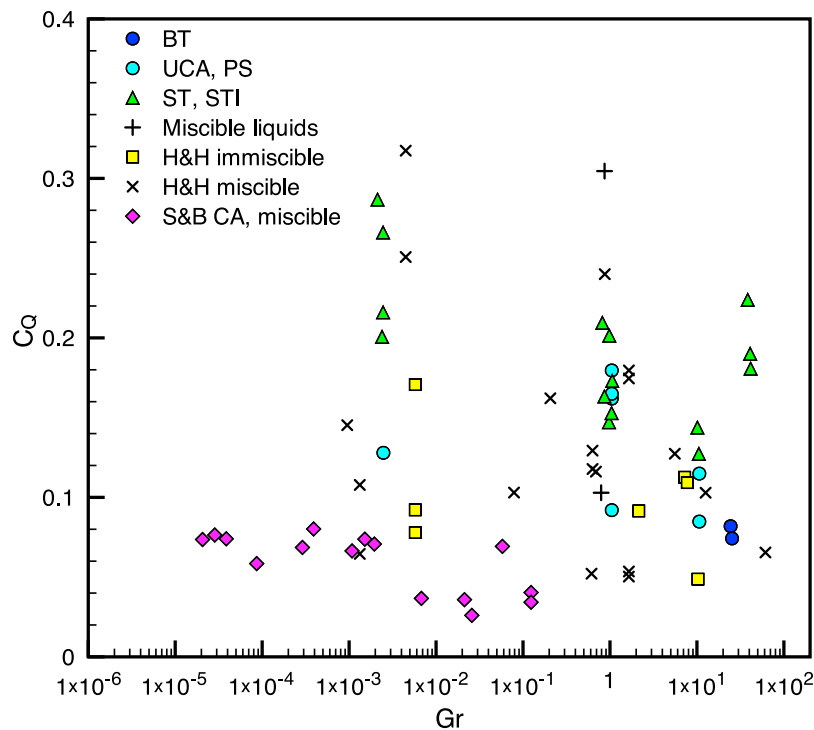


**Figure 9.** Variation of the flux coefficient with the Grashof number and flow pattern for experiments with Gr < 100. Nomenclature, BT: blobs and/or turbulent flow in vertical pipes; UCA,PS: unsteady core-annular or pseudo-stratified flow in vertical pipes; ST, STI: stratified flow with or without instabilities in inclined pipes; CA: core-annular flow; H&H: *Huppert and Hallworth* [2007]; S&B: *Stevenson and Blake* [1998].

mixture at low and high strain rates, where the former is equivalent to the Einstein-Roscoe relation (equation (10)). Recently, *Costa et al.* [2009] and *Ishibashi* [2009] have developed models that account for the non-Newtonian behavior of high-concentration mixtures at different strain rates. Since our steady state model of convection depends only on two viscosities (source and sinking magmas), and given the variability in the estimation of the relative viscosity of the mixture from the models, we adopted the Einstein-Roscoe relation.

## 4.2. Constraints on the Amount and Rate of Degassing

[34] The degassing rate can be quantified by combining the emission rate of outgassed $SO_2$, measured with remote sensing techniques [*Symonds et al.*, 1994], and the composition and concentration of volatiles in the melt as measured in glass inclusions trapped in phenocrysts (petrologic method) [e.g., *Kazahaya et al.*, 1994; *Gerlach et al.*, 1996]:

$$Q_m = 10^2 \frac{M_{(S)}}{M_{(SO_2)}} \frac{Q_{SO_2}}{\Delta S} \qquad (11)$$

where $Q_m$ [$kg/s$] is the magma degassing rate, $\Delta S$ [wt%] is the sulfur lost from the melt, $M_{(S)} = 32.066$ [$g/mol$] and $M_{(SO_2)} = 64.065$ [$g/mol$] are the molecular mass of sulfur and sulfur dioxide, respectively ($M_{(SO_2)}/M_{(S)} \simeq 2$), and $Q_{SO_2}$ [$kg/s$] is the emission rate of $SO_2$ measured at the surface. The magma degassing rate, $Q_m$, is equivalent to the mass of magma that looses a $\Delta S$ amount of sulfur per unit time, with the assumption that this gas is homogeneously distributed within the magma.

[35] The outgassed sulfur $\Delta S$ is obtained from measurements of $S$ concentrations in glass inclusions and in matrix glass of lava or scoria samples, that represent the volatile content of the relatively volatile-rich and degassed magmas, respectively:

$$\Delta S = S_{gi}(1 - X_{gi}) - S_{mg}(1 - X_{mg}) \qquad (12)$$

with $S_{gi}$ [wt%] the concentration of sulfur measured in the glass inclusion and $S_{mg}$ [wt%] the concentration of sulfur in the matrix glass of the sample. $X_{gi}$ and $X_{mg}$ correspond to the mass fractions of crystals at the times of melt inclusion formation and quenching of the matrix glass of the scoria or lava sample, respectively. If the crystal fractions in equation (12) are unknown, they can be estimated from the enrichment of a highly incompatible element in the glass with respect to the whole rock [*Self et al.*, 2008]. Let $I$ be the concentration of an

incompatible element, then equation (12) can be expressed as:

$$\Delta S = I_{wr}\left(\frac{S_{gi}}{I_{gi}} - \frac{S_{mg}}{I_{mg}}\right) \qquad (13)$$

where the subscript *wr* refers to the whole rock composition and $I$ is expressed in wt% or wt-fraction. Here it is assumed that crystallization of a sulfide or any other phase that includes $S$ is negligible or absent. Major oxides such as $TiO_2$ or $K_2O$ as well as incompatible trace elements such as Zr are candidates to replace $I$ in equation (13). For instance, $TiO_2$ has been used by *Self et al.* [2008] and *Blake et al.* [2010] in tholeiitic basalts to study degassing in flood-basalt eruptions.

[36] The volume flow rate $Q_v$ [$m^3/s$] of the ascending volatile-rich magma can then be calculated by dividing the magma degassing rate ($Q_m$), obtained from equation (11), by the density of the ascending magma ($\rho_a$). Combining this definition with equations (6) and (11), the following expression is obtained:

$$Q_m = 50\frac{Q_{SO_2}}{\Delta S} = \Gamma \frac{C_Q}{\mu_d}\rho_a\Delta\rho \qquad (14)$$

with

$$\Gamma = gR^4 \cos\theta \qquad (15)$$

a factor with units [$m^5/s^2$] that depends on the geometry of the system only. Thus, from the measurements of emission rates of $SO_2$ and sulfur loss ($\Delta S$), along with the properties of the magma, the value of $\Gamma$ can be calculated. Then, using equation (15) and for a given value of $\theta$, the equivalent radius $R$ is obtained. Changes in the magma emission rate ($Q_{SO_2}$) may reflect changes in magma volatile content ($\Delta S$) and properties ($\rho_a$, $\rho_d$, $\mu_d$), and/or changes in equivalent radius of the conduit ($R$). We now apply this to the specific case of Villarrica volcano, Chile.

## 4.3. Degassing at Villarrica Volcano

[37] Villarrica is a stratovolcano located in southern Chile that exhibits persistent degassing activity from a lava lake located inside its crater [*Calder et al.*, 2004; *Palma et al.*, 2008]. The eruptive activity observed at Villarrica volcano within the last century is summarized as follows [*Casertano*, 1963; *Petit-Breuilh*, 1994]: (1) lava flows from the main crater or fissures in the upper part of the cone, in association with explosive activity at the summit (e.g., in 1963, 1984); (2) agitated lava lakes with

strombolian explosions (e.g., in 1948); (3) violent explosions from summit generating high eruption columns (in 1908, 1948, 1964, 1971); and (4) high and sustained lava fountains at the summit (in 1908, 1964, 1971). Since the last eruption in 1984, the activity has been limited to the crater area and characterized by the emission of a gas plume associated with mild explosive outgassing from the lava lake. It has been suggested that the upper plumbing system of Villarrica consists of a near-vertical conduit with a length greater than 2000 m, and that convection of magma within this conduit is the most appropriate model that explains the open-vent degassing activity [*Witter et al.*, 2004; *Palma et al.*, 2008].

### 4.3.1. Sulfur Loss and Degassing Rate

[38] As shown by equation (11), given a fixed value of $SO_2$ emissions, the higher the amount of sulfur loss (equations (12) or (13)) the smaller the magma degassing rate. Thus, considering a fixed concentration of sulfur in the degassed magma, the lower limit for $Q_m$ can be obtained from the highest concentration of S measured in glass inclusions. Melt inclusion data for Villarrica are given by *Witter et al.* [2004] and J. A. Cortés et al. (A comparative study of recent products from Villarrica volcano, Chile: A quiescently degassing basaltic arc system with a violent explosive history, submitted to Bulletin of Volcanology, 2011) and shown in Figure 10. *Witter et al.* [2004] reported data from samples erupted in 2000 where the maximum concentration of S reached 0.092 wt% in a glass inclusion trapped in olivine at >1000 bars. Cortés et al. (submitted manuscript, 2011) found glass inclusions in samples from 1971 with up to 0.12 wt% of sulfur. Much lower sulfur abundances (~0.04 wt%) in other glass inclusions from 2000 and 1971 indicate variable degrees of degassing before entrapment (Figure 10a). All other samples show high degrees of degassing, with sulfur abundances lower than 0.02 wt% and low $S/TiO_2$ ratio. Matrix glass of scoria samples from 2000 have concentrations of ~0.01 wt% of sulfur [*Witter et al.*, 2004].

[39] The highest $S/TiO_2$ ratio is found in one glass inclusion from 2000 and another one from 1984, with values 0.08 and 0.078, respectively (Figure 10b). These samples also have similar $S/Cl$ and $S/K_2O$ ratios, which suggests that they represent melts that have not degassed to different degrees. Despite having greater S concentrations, glass inclusions from 1971 have a lower $S/TiO_2$ ratio with an average

of 0.058 (in a group of five samples, and with a maximum of 0.063), supporting the idea that these relatively evolved inclusions (also with slightly higher $TiO_2$ and lower magnesium number) were trapped after degassing had commenced. It is noteworthy that the amount of $TiO_2$ in the whole rock (~1.22 wt%) is slightly greater than that of some glass inclusions (Figure 10). This may be due to differences in analytical techniques (XRF versus EMP), imperfectly incompatible nature of Ti, or because of the open volcanic system in which some crystals have been picked up from a more primitive magma or partly crystalline rock within the plumbing system.

[40] A summary of the values used here for the calculation of the sulfur loss and magma degassing rate is presented in Table 3. Three possible scenarios are considered for the initial sulfur content: (1) with the maximum concentration of S obtained from the 1971 data (0.12 wt% S), (2) with the volatile-rich inclusion in a sample from 2000 (0.09 wt% S), and (3) with the high-S but relatively degassed glass inclusions from 2000 (0.04 wt% S). The results show that sulfur loss within the upper part of the plumbing system at Villarrica ranges from 0.029 to 0.107 wt% for initial S contents of 0.04 and 0.12 wt%, respectively.

[41] The emission rate of $SO_2$ used here corresponds to the average gas emission measured by *Witter et al.* [2004] in 2000 (2.8 kg/s), during which time the samples with glass inclusions were erupted. This corresponds to a period of background degassing at Villarrica [*Palma et al.*, 2008]. Calculation of the magma degassing rate results in 1310–4853 kg/s, with the highest value associated with the lowest initial content of sulfur and sulfur loss (Table 3).

### 4.3.2. Equivalent Radius and Magma Ascent Rate

[42] Water concentrations used in the calculations (Table 3) were chosen according to the initial content of sulfur in the magma. Because of the large uncertainty in the measurements of water in glass inclusions [*Witter et al.*, 2004], the ratio between these two species is not well constrained. Nevertheless, based on the composition of the glass inclusions and the volatile ratio based on direct sampling of the volcanic plume [*Shinohara and Witter*, 2005], these values are considered reasonable. The densities and viscosities of the ascending magma were calculated using the whole-rock composition of reticulite and scoria from 2000 at 1200°C
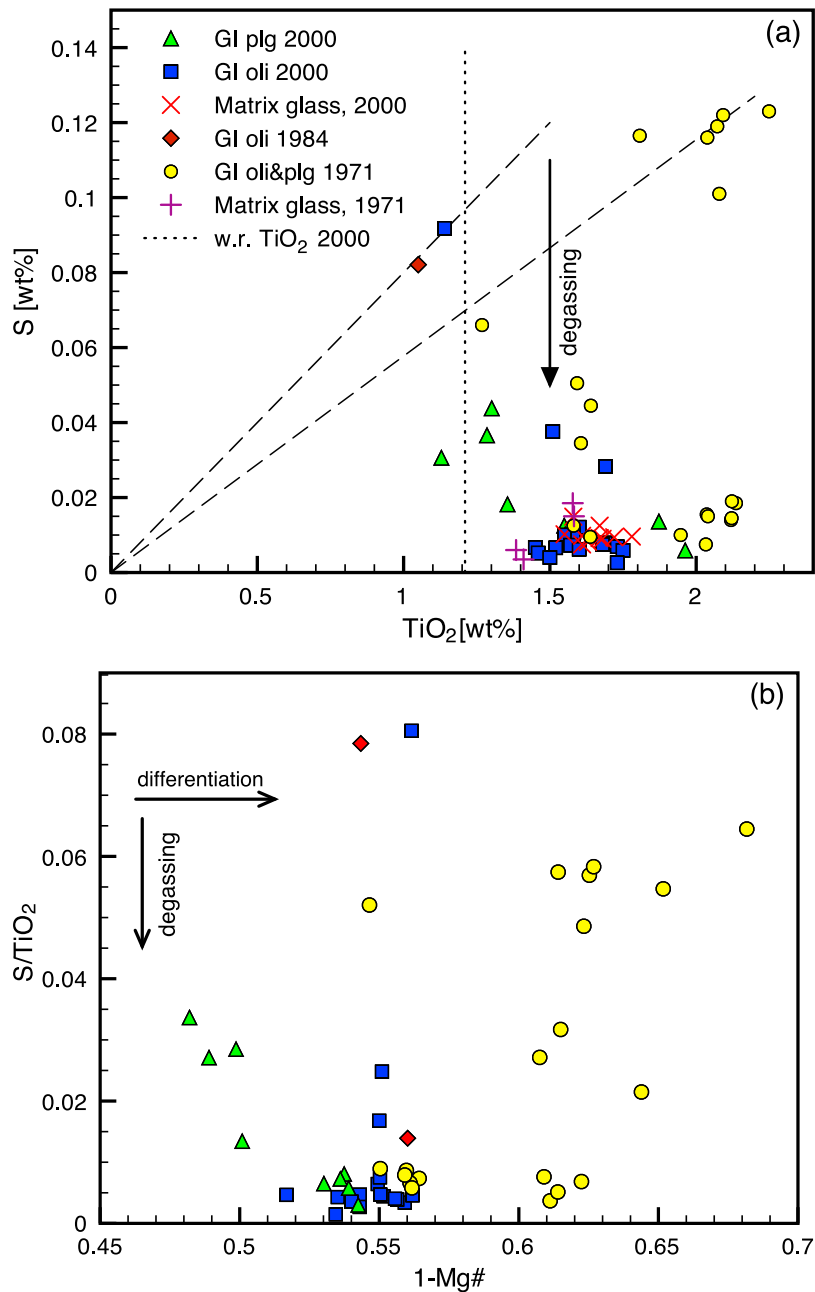
**Figure 10.** (a) Concentration of sulfur and TiO$_2$ in glass inclusions hosted in olivine and plagioclase, and the composition of matrix glass from reticulite erupted in 2000 at Villarrica volcano. One glass inclusion in olivine from a lava flow in 1984 is also shown. The whole-rock value of TiO$_2$ is used to qualify degrees of fractionation between samples. Dashed lines represent constant S/TiO$_2$ ratio. (b) Plot of the magnesium number (Mg#, molar MgO/(MgO+FeO*)) versus the mass ratio between sulfur and TiO$_2$ for glass inclusions from 1971, 1984 and 2000. Data from 2000 and 1984 are from *Witter et al.* [2004] and data from 1971 are from Cortés et al. (submitted manuscript, 2011).

and 100 MPa. For the density and viscosity of the descending magma we used the composition of the matrix-glass reticulite from 2000 at 1100°C and 10 MPa. It is worth noting that the crystal content of the tephra samples was re-calculated based on modal composition of minerals present, yielding a concentration of 28.5 wt% (23.6 wt% plagioclase

and 4.9 wt% olivine), much lower than that reported by *Witter et al.* [2004].

[43] For the three scenarios analyzed here the density variation is dictated by the water and crystal content in the ascending magmas, with values of 168, 136 and 62 kg m$^{-3}$ for scenarios 1, 2 and 3,

Geochemistry Geophysics Geosystems G³

**Table 3.** Summary of the Values Used in the Calculation of the Sulfur Loss, $\Delta S$, Degassing Rate of the Magma, $Q_m$, Magma Ascent Rate, $Q_v$, Equivalent Radius, $R$, Viscosity Ratio, $\kappa$, and Grashof Number, $Gr$[a]

| | Units | Descending Magma ($mg\ d$) | Ascending Magma ($gi$, $a$) (1) | (2) | (3) |
|---|---|---|---|---|---|
| $S_{mg,gi}$ | wt% | 0.01 | 0.12 | 0.09 | 0.04 |
| $TiO_2$ | wt% | | 1.28 | 1.28 | 1.36 |
| $X_{mg,gi}$ | wt frac. | 0.285 | 0.05 | 0.05 | 0.1 |
| $\Delta S$ | wt% | | 0.107 | 0.078 | 0.029 |
| $Q_{SO2}$ | kg s$^{-1}$ | | 2.8 | 2.8 | 2.8 |
| $Q_m$ | kg s$^{-1}$ | | 1310 | 1787 | 4853 |
| $H_2O$ | wt% | 0.1 | 2 | 1.5 | 0.5 |
| $\mu_{d,a}$ | Pa s | $3.61\cdot10^4$ | $1.72\cdot10^1$ | $3.13\cdot10^1$ | $2.77\cdot10^2$ |
| $\rho_{d,a}$ | kg m$^{-3}$ | 2692 | 2524 | 2556 | 2630 |
| $Q_v$ | m$^3$ s$^{-1}$ | | 0.52 | 0.70 | 1.85 |
| $\Delta\rho$ | kg m$^{-3}$ | | 168 | 136 | 62 |
| $\Gamma$ | m$^5$ s$^{-2}$ | | 1115 | 1856 | 10743 |
| $R$ | m | | 3.3 | 3.7 | 5.8 |
| $\kappa$ | | | $4.8\cdot10^{-4}$ | $8.7\cdot10^{-4}$ | $7.7\cdot10^{-3}$ |
| $Gr$ | | | 0.12 | 0.14 | 0.24 |

[a]$X$ is crystal content of the magma and the subscripts $gi$ and $mg$ represent the times of glass inclusion entrapment (for the ascending magma) and quenching of the matrix (for the descending magma), respectively. $TiO_{2,gi}$ and $X_{gi}$ are related by the equality $TiO_{2,wr}/TiO_{2,gi} = (1 - X_{gi})$. Subscripts $a$ and $d$ in density and viscosity also refer to the ascending and descending magmas, respectively. $Q_{SO2}$ is the sulfur dioxide emission rate measured at the surface in 2000. Other values used in the calculations are $C_Q = 0.1$, $\theta = 0$.

respectively (Table 3). Calculation of the volume flow rate of magma ascent yields a range from 0.52 to 1.85 m$^3$ s$^{-1}$, where the limits correspond to the scenarios with highest and lowest initial sulfur, respectively. Note the inverse relationship between the density difference and magma flow rate, which results from the higher magma degassing rate (and consequently higher value of $\Gamma$) in the case with lower initial content of sulfur and density difference (see equation (14)). The conduit equivalent radius ranges from 3.3 to 5.8 m (Table 3), with the widest conduit associated with the highest magma ascent rate. For comparison, *Witter et al.* [2004] estimated conduit radii of 2.7 and 2.1 m associated with ascending magmas with water contents of 1 and 4 wt%, respectively.

### 4.3.3. Implications for the Observed Variations of Gas Emissions

[44] Gas measurements at Villarrica have been measured sporadically since 1999 [*Calder et al.*, 2004; *Witter et al.*, 2004; *Palma et al.*, 2008]. *Palma et al.* [2008] showed that emissions of sulfur dioxide from Villarrica range from about 1.2 to 15 kg s$^{-1}$ (daily mean values collected between 2000 and 2006), with variations of up to 8 kg s$^{-1}$

observed over just a few days. Note that the analysis carried out above used an emission rate of 2.8 kg s$^{-1}$ (Table 3). Re-arranging equation (14) provides an expression for the emission rate of sulfur dioxide:

$$Q_{SO_2} = c_1 \frac{\rho_a \Delta\rho}{\mu_d} \Delta S \tag{16}$$

with

$$c_1 = \Gamma \frac{C_Q}{50} = 0.02 C_Q R^4 g \cos\theta \tag{17}$$

a parameter that depends on the equivalent radius. For example, for a vertical conduit with an equivalent radius of 4.75 m the value of $c_1$ is about 10. Following equation (16), variations in observed gas emissions can now be explained by (1) changes in the size of the conduit, (2) variations in the volatile concentration of the magma, or (3) changes in the efficiency of degassing by another mechanism. An increase in $Q_{SO_2}$ from 1.2 to 15 kg s$^{-1}$ due to a change in the conduit size alone requires a variation of the equivalent radius by a factor of $(1.5/1.2)^{1/4} = 1.9$. This change seems somewhat unreasonable given that it refers to a change of the equivalent radius of the whole conduit and that gas emission rates were only elevated for a period of a few days in 2005 after which they returned to the established background. Actually, in a basaltic open-vent system such as Villarrica, which exhibits month- to year-long variations in gas emissions and activity at the crater [*Palma et al.*, 2008], it is likely that the geometry and size of the plumbing system remain relatively unchanged. Thus, for a given radius the parameter $c_1$ in equation (17) is assumed constant. Then, using equation (16) the variations in gas emissions can be investigated based on different volatile contents of the magma and its physical properties.

[45] Increasing the emissions of sulfur dioxide while keeping the equivalent radius constant can be achieved by increasing the volatile content of the magma at depth (Figure 11). However, an increase in $Q_{SO_2}$ can also be achieved by increasing the volatile content retained in the degassed magma, even though this has the effect of decreasing both the volatile loss and the density difference (see equation (16)). This counter-intuitive result is explained by the significant decrease in viscosity of the degassed magma associated with higher volatile contents (Table 4), which in this case determines a higher efficiency of degassing by convection in
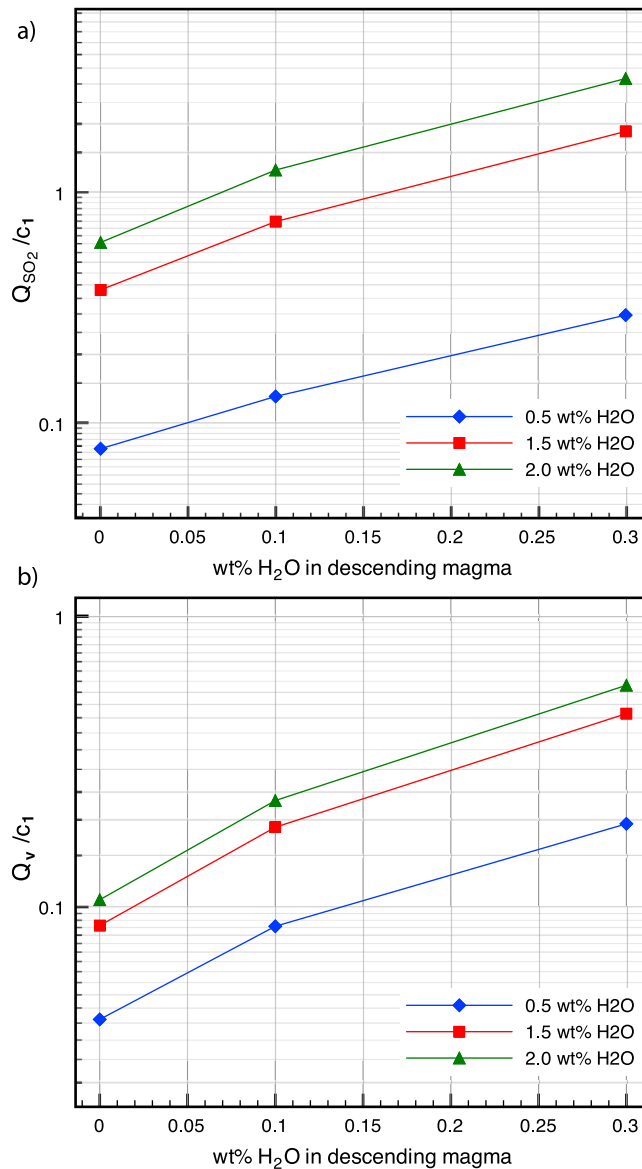
**Figure 11.** Variations in emission rates of $SO_2$ and magma flow rate, for a plumbing system of any size and geometry, as a function of the volatile content of the ascending and descending magmas (see values in Table 4). Each curve represents an ascending magma with a determined water content. Here $c_1$ is an undetermined constant; for example, for a vertical conduit with an equivalent radius of 4.75 m the value of $c_1$ is about 10. The analysis was not extended beyond 0.3 wt% of $H_2O$ in the descending magma because the water content in the matrix glasses from Villarrica are characteristically low [*Witter et al.*, 2004].

**Table 4.** Plausible Values of Volatile Concentration, Density and Viscosity of Magmas at Villarrica[a]

|  | Units | Descending Magma | | | Ascending Magma | | |
|---|---|---|---|---|---|---|---|
| $H_2O$ | wt% | 0 | 0.1 | 0.3 | 0.5 | 1.5 | 2 |
| S | wt% | 0 | 0.01 | 0.01 | 0.04 | 0.09 | 0.12 |
| X | wt frac. | 0.285 | 0.285 | 0.285 | 0.1 | 0.05 | 0.05 |
| $\rho$ | kg m$^{-3}$ | 2697 | 2692 | 2683 | 2630 | 2556 | 2524 |
| $\mu$ | Pa s | $8.2 \cdot 10^4$ | $3.6 \cdot 10^4$ | $1.4 \cdot 10^4$ | $2.8 \cdot 10^2$ | $3.1 \cdot 10^1$ | $1.7 \cdot 10^1$ |

[a]These values are used to explore the variations in gas emissions and magma convection rate as shown in Figure 11.

terms of the magma flow rate, $Q_v$ (Figure 11). Note that unlike the values of $Q_v$ in Table 3, the volumetric rates of magma convection in Figure 11 were calculated for a unique equivalent radius. The variation in volatile content of the magma that produces an increase in $Q_{SO_2}$ from 1.2 to 15 kg s$^{-1}$ (about 14 units) depends on the size of the conduit, and thus $c_1$ (equations (16)–(17)). If, for instance, $c_1 = 10$ then taking the lowest value of gas emissions given by an ascending melt with 0.5 wt% $H_2O$ and a dry descending magma ($Q_{SO_2}/c_1 = 0.08$, Figure 11), the new degassing conditions would require much higher volatile contents in both magmas, so that $Q_{SO_2}/c_1 = 0.08 + 14/c_1 = 1.48$. Thus, the relationship

in equation (16) establishes constraints on the size of the conduit and variations in volatile contents of the magma. When these variations are known, this information can be combined with petrologic data in order to estimate the equivalent radius. When the equivalent radius and the volatile content as well as physical properties of the descending magma are known, then variations in gas emissions measured at the surface give insights on the changes in the volatile content of the magma ascending to the surface.

[46] From the three scenarios of magma degassing analyzed above (Table 3), and given the equivalent radius derived for each case, changes in the initial gas content and density of the ascending magma have been used to explore the variation in $Q_{SO_2}$ (Figure 12). The results show that with the two smallest radii gas emissions are lower than 5 kg s$^{-1}$ in all three cases, and that in order to reach greater amounts similar to those measured at Villarrica the initial sulfur content would have to reach values much greater than those considered here. With an equivalent radius of 5.8 m, however, large variations of sulfur-dioxide emission rates can be achieved which include those observed at Villarrica. Indeed, $SO_2$ emissions of 15 kg s$^{-1}$ are reached by changing
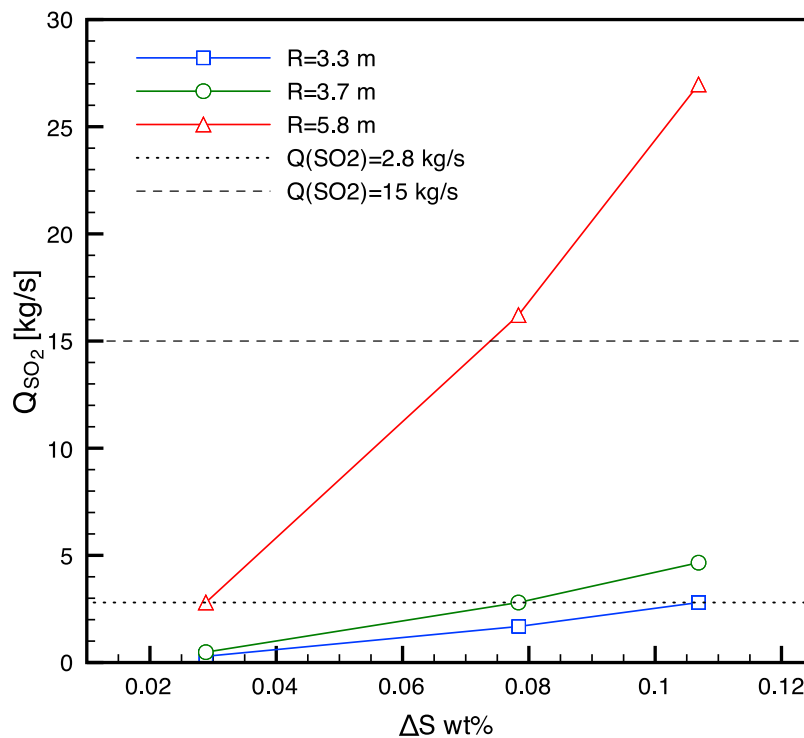


**Figure 12.** Expected emission rates of sulfur dioxide given the variations of sulfur loss for three equivalent radii (3.3, 3.7 and 5.8 m). The symbols show analyzed cases of sulfur loss with $Q_{SO_2} = 2.8$ kg s$^{-1}$ as well as predicted $SO_2$ emissions for all values of sulfur loss given a specified radius (Table 3). A higher $SO_2$ emission rate of 15 kg s$^{-1}$, measured in January 2005 by *Palma et al.* [2008] is also shown; this amount of gas emission is only reached with the calculated equivalent radius of 5.8 m.

the conditions from the relatively low initial gas content (scenario 3) to intermediate gas contents (scenario 2), both measured in samples from 2000. This result is a consequence of the strong dependency of the magma flow rate on the radius of the conduit (see equations (6) and (16)). In other words, a greater conduit size favors more efficient convection and magma degassing. Therefore, the scenario that best explains the degassing observed during 2000 at Villarrica volcano, and its variations during the following years, corresponds to that of a partially degassed magma with initial gas concentrations of ~0.04 wt% S (0.5 wt% $H_2O$) ascending within a plumbing system with equivalent radius of ~5.8 m. Emissions of sulfur dioxide as great as 15 kg s$^{-1}$ can be produced by the ascent of a relatively volatile-rich magma containing ~0.09 wt% S (1.5 wt% $H_2O$).

## 5. Conclusions

[47] Convection of magma within the plumbing system of many basaltic open-vent volcanoes is considered the driving mechanism of persistent outgassing. A simple model has been considered in which volatile-rich magma ascends from a reservoir to the surface within dikes or cylindrical conduits, whereas degassed magma sinks within the same conduit back down to the reservoir. New laboratory experiments of convection of immiscible fluids in vertical and tilted pipes show that, for a given pair of fluids and regardless of the flow pattern, the volumetric flow rate stays constant throughout the experiment. However, the value of the volume flow rate is affected by the flow pattern. Flow patterns other than core–annular flow actually yielded higher flow rates, which is particularly significant because this pattern has been the one typically assumed by the community in the analysis of these systems. When the two–fluid flow became stratified in experiments with tilted pipes the volume flow rate increased. It was found that the Grashof number defines two groups with different convection rates. For $Gr < 100$ the value of the flux coefficient remains constant for all Reynolds numbers and its variation depends essentially on the physical properties of the fluids and flow pattern. Convection rates of miscible fluids fall within the range values of immiscible fluids. In this group the flux coefficient is used to calculate the volume flow rate. For vertical conduits the flux coefficient can be approximated as 0.1, and for inclined conduits it can be approximated as 0.2. For $Gr > 100$ the volume flow rate is determined by a constant Froude number. In this case

convection rates obtained with miscible fluids can be much lower than that obtained for immiscible fluids because of mixing.

[48] The model of magma convection developed here allows the calculation of the equivalent radius, a parameter that constrains the dimensions of the plumbing system, and which determines the relationship between gas concentration in the source magma (at depth) and gas emission rates measured at the surface. Calculation of the convective flow rate requires knowledge of the equivalent radius and some properties of the ascending and descending magmas. In particular, the volume flow rate increases with higher density difference between the magmas and it is highly influenced by the large variations in viscosity of the degassed magma as it changes its volatile content and crystallinity. The equation for calculating the volumetric flow rate was combined with the petrologic method in order to obtain the relationship between convection rate and the variation in volatile content of the magmas. The model of convection was applied to Villarrica volcano. An estimation of the magma degassing rate, magma flow rate, equivalent radius and Grashof number, among other parameters, were calculated for Villarrica magma for three initial volatile contents. With the lowest value of initial sulfur (0.04 wt% S, equivalent to 0.5 wt% $H_2O$) the magma degassing rate and equivalent radius obtained were the highest. It also yielded the most realistic relation between $SO_2$ emission rates and sulfur loss, in which changes in initial sulfur content from 0.04 to 0.09 wt% S (~1 wt% $H_2O$) can explain the increase in $Q_{SO_2}$ from the background 2.8 kg s$^{-1}$ measured in 2000 to 15 kg s$^{-1}$ as measured during the elevated activity in 2005.

[49] The analysis of convection presented herein can be applied to other volcanic or intrusive settings where there is bidirectional flow through narrow conduits. This model provides possibilities for studying the causes and consequences, in terms of varying magma composition and volatile content, of changes in the outgassing activity at open-vent volcanoes.

## Appendix A: Steady State Countercurrent Flow in Narrow Conduits
### A1. Core-Annular Flow in a Vertical Pipe

[50] Here we consider, from an analytical point of view, the characteristics of steady core–annular flow in a vertical pipe. This is followed by a dimensional
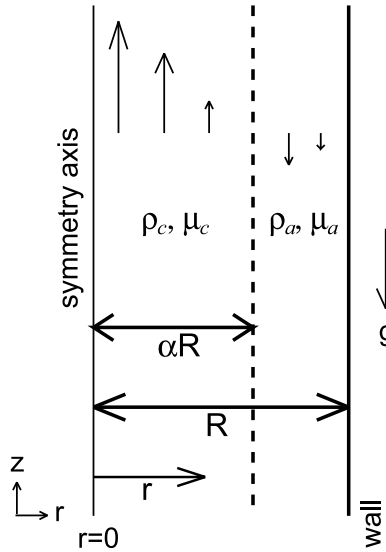
**Figure A1.** Definition of the geometry in cylindrical coordinates and the parameters for the problem of laminar convection in a vertical tube.

analysis of the problem and the specification of dimensionless coefficients.

[51] First, we consider the problem of two-fluid viscous laminar flow within a vertical cylindrical tube under steady state conditions. The geometry and variables of the problem are shown in Figure A1. It is necessary to specify a tube length which is large compared to the tube radius, so that end-effects are unimportant and not considered. Only Newtonian fluids with constant viscosity and density are considered (isothermal). Surface tension effects are neglected. An axisymmetric solution where one fluid flows inside (inner fluid) and the other flows next to the wall (outer fluid) and surrounding the inner fluid is assumed. The following formulation is valid only in the case of flow of immiscible and incompressible fluids.

[52] In cylindrical coordinates, the general solution of the Navier-Stokes equations under the previous assumptions is [e.g., *Batchelor*, 1967; *Hickox*, 1971]:

$$v(r) = -\frac{P}{4\mu}r^2 + C_1 \ln r + C_2 \qquad (A1)$$

where $v$ is the vertical velocity, $r$ the radial distance, $P = -dp/dz - \rho g$ is the combination of pressure gradient and gravitational force per unit length, and $\mu$ is the viscosity of the fluid. The constants $C_1$ and $C_2$ need to be determined by using the appropriate boundary conditions.

[53] In the two-fluid problem the solution of equation (A1) is obtained separately for both fluids

considering the following boundary conditions: the velocity of the inner fluid is finite at the cylindrical axis ($v(r = 0) < \infty$), continuity of shear stresses and velocity across the interface, and zero velocity of the outer fluid at the wall. Hence, the velocity profile for the two-fluid problem becomes

$$v_c(r) = \left[\frac{\Delta p}{h} - \rho_c g\right] \frac{(\alpha R)^2 - r^2}{4\mu_c} + v_a(\alpha R) \qquad (A2)$$

$$0 \le r \le \alpha R$$

$$v_a(r) = \left[\frac{\Delta p}{h} - \rho_a g\right] \frac{R^2 - r^2}{4\mu_a} - \frac{\Delta \rho g}{2\mu_a}(\alpha R)^2 \ln\left(\frac{r}{R}\right) \qquad (A3)$$

$$\alpha R \le r \le R$$

where the subscripts $c$ and $a$ refer to the core and annular fluids, respectively, $\mu$ is the viscosity, $\rho$ the density, $R$ is the radius of the cylinder, $\alpha R$ is the radius of the core fluid flow and defines the position of the interface, $\Delta \rho = \rho_a - \rho_c$ is the density difference, $\Delta p = p_b - p_t$ is the difference between the pressure at the bottom and top of the fluid column, $h$ the depth (length) of the column, and $g$ is the absolute value of gravity. The first term in the right-hand side of equations (A2) and (A3) is the Hagen-Poiseuille velocity for the corresponding radial section of the cylinder. Hence, the core fluid is the only one that develops such a velocity profile.

[54] The unknown pressure gradient has been previously modeled by two approximations: (1) by setting the position of the interface ($\alpha$) at 0.6 of the radius, and (2) with the value that maximizes the flow rate. The first approximation is based on the experimental results of *Stevenson and Blake* [1998]. The second approximation has been considered in models of lubricating pipelines of water and oil [*Joseph and Renardy*, 1993b], and it has been proposed by *Huppert and Hallworth* [2007] to explain their experimental results. Neither of these approximations is actually consistent with the position of the interface observed in laboratory experiments.

[55] The pressure drop is expressed here as a combination of the weights of the individual fluids in the cylinder,

$$\Delta p = [\phi \rho_a + (1 - \phi)\rho_c]gh \qquad (A4)$$

where $\phi$ is a parameter that represents the fluid weight fraction of the annular fluid.

[56] Assuming that this two-fluid flow is a consequence of convection within the cylinder with no loss of mass, and with interminable availability and
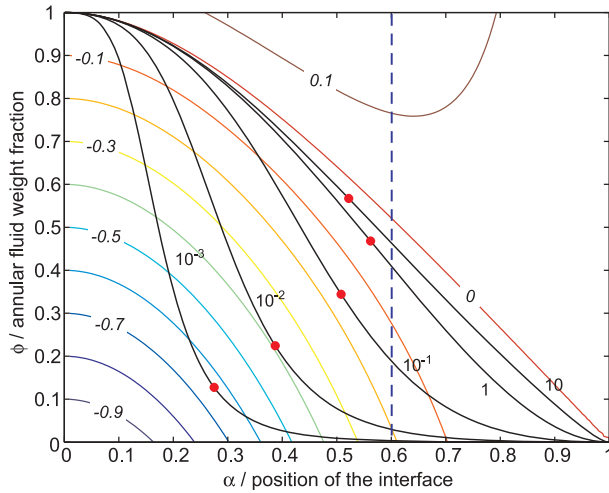
**Figure A2.** Solution of equation (A8) for different values of the viscosity ratio, $\eta = 10^{-3}, 10^{-2}, 10^{-1}, 10^0, 10^1$ (solid dark lines). The plot shows the contour lines of the dimensionless volumetric flux $\widehat{Q}_a$ (equation (A12)) for values between $-0.9$ and $0.1$. The dots represent the values that maximize the volumetric flux, and the vertical dashed line constrains the solution when the position of the interface is at $\alpha = 0.6$.

influx of the two fluids at both ends of the tube, the volume of the system must be conserved:

$$Q_c + Q_a = 0 \qquad (A5)$$

where $Q_c$ and $Q_a$ are the volumetric flow rates of the fluids in the core and annulus, respectively. $Q_c$ is given by

$$Q_c = \int_0^{2\pi} \int_0^{\alpha R} v_c(r) r \, dr \, d\theta$$
$$= \frac{\pi(\alpha R)^4}{8\mu_c} \left[ P_c + 2\eta P_a \frac{(1-\alpha^2)}{\alpha^2} - 4\eta(P_c - P_a) \ln\alpha \right] \quad (A6)$$

where $\eta = \mu_c/\mu_a$ is the viscosity ratio between the fluids in the core and annulus (note that this is different to the viscosity between the lighter and heavier fluids used in the main part of the text), and $Q_a$ is given by

$$Q_a = \int_0^{2\pi} \int_{\alpha R}^{R} v_a(r) r \, dr \, d\theta$$
$$= \frac{\pi R^4}{8\mu_a} \left[ P_a(1-\alpha^2)^2 + 2(P_c - P_a)\alpha^2(1 - \alpha^2 + 2\alpha^2\ln\alpha) \right] \qquad (A7)$$

Combining equations (A5)–(A7) and using $\phi$ to represent the pressure gradient (equation (A4)), we get

$$\phi = \frac{2\alpha^2 - \alpha^4 - 1}{(1 - \eta^{-1})\alpha^4 - 1} \qquad (A8)$$

which is independent of the fluid densities. Hence, the position of the interface only depends on the viscosity ratio of the fluids, but varies with the pressure drop along the cylinder.

[57] The solution to this equation is shown in Figure A2. It is worth noticing that the volumetric fluxes of the uprising and sinking fluids (equations (A6) and (A7)) are different to the expressions presented by *Kazahaya et al.* [1994] that assume Hagen-Poiseuille flow for both fluids with zero velocity at the interface.

[58] The expressions of the volumetric flux (equations (A5)–(A7)) are now re-arranged to obtain the following dimensionless parameters:

$$Q_c = \widehat{Q}_c Q^*, \qquad Q_a = \widehat{Q}_a Q^* \qquad (A9)$$

with

$$Q^* = \frac{\pi}{8} \frac{R^4 g \Delta\rho}{\mu_a} \qquad (A10)$$

$$\widehat{Q}_c(\phi, \alpha, \eta) = \alpha^4 \left[ \frac{\phi}{\eta} - 2(1-\phi)\left(\frac{1-\alpha^2}{\alpha^2}\right) - 4\ln\alpha \right] \quad (A11)$$

$$\widehat{Q}_a(\phi, \alpha) = (\phi - 1)(1 - \alpha^2)^2 + 2\alpha^2(1 - \alpha^2) + 4\alpha^4 \ln\alpha \qquad (A12)$$

where $\widehat{Q}_c$ and $\widehat{Q}_a$ represent the normalized volumetric flux (both dimensionless) of the fluids in the core and annulus, respectively, which preserve the condition of mass and volume conservation, $\widehat{Q}_c + \widehat{Q}_a = 0$.

## A2. Laminar Flow in a Slot

[59] In this section we show the problem of a vertical slot with co-axial and symmetric flow on a center plane parallel to the walls. The walls are separated by a distance $W$ and have a length $L$. The details of the geometry and the parameters involved in the following model are shown in Figure A3. This configuration is similar to the axisymmetric fluid flow in a cylinder, thereby a similar solution is expected.

[60] The Hagen-Poiseuille solution for a vertical slot with only one fluid is:

$$v(x) = -\left(\frac{dp^*}{dz}\right)\frac{A^2 - x^2}{2\mu} \qquad (A13)$$
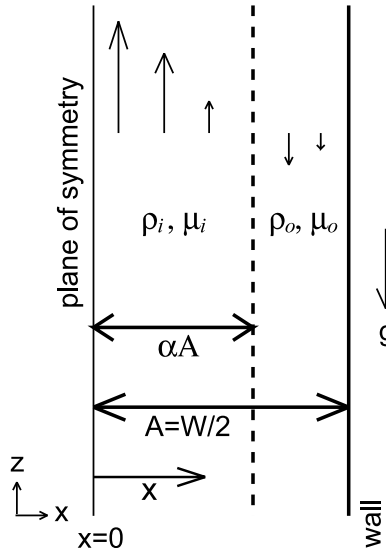
**Figure A3.** Definition of the geometry and parameters for the problem of laminar convection in a vertical slot.

where $p^* = p + \rho\, gz$ is the piezometric pressure, $A = W/2$ half width of the slot, and $\mu$ the viscosity of the fluid. With two fluids flowing with the configuration depicted in Figure A3, the velocity profile is given by:

$$v_i(x) = \frac{P_i}{2\mu_i}\left((\alpha A)^2 - x^2\right) + v_o(\alpha A) \qquad (A14)$$
$$0 \le x \le \alpha A$$

$$v_o(x) = \frac{P_o}{2\mu_o}\left(A^2 - x^2\right) + (\alpha A)\frac{(P_i - P_o)}{\mu_o}(A - x)$$
$$\alpha A \le x \le A. \quad (A15)$$

[61] The volumetric flux is given by:

$$Q_i = \frac{2}{3}L\frac{P_i}{\mu_i}(\alpha A)^3 + L\frac{A^3\alpha}{\mu_o}\left(P_o(1-\alpha)^2 + 2\alpha P_i(1-\alpha)\right) \qquad (A16)$$

$$Q_o = \frac{2}{3}L\frac{P_o}{\mu_o}A^3 - L\frac{\alpha A^3}{\mu_o}$$
$$\cdot \left[\frac{2}{3}P_o\left(1+\alpha^2\right) - P_i\left(1+\alpha^2\right) + 2(P_i - P_o)\alpha\right]. \quad (A17)$$

[62] Using the definition of the pressure drop as a given weight of fluid (equation (A4)), the volumetric flux becomes:

$$Q_i = \widehat{Q}_i Q_s, \qquad Q_o = \widehat{Q}_o Q_s \qquad (A18)$$

with

$$Q_s = \frac{2L}{3A}\frac{A^4 g\Delta\rho}{\mu_o} \qquad (A19)$$

$$\widehat{Q}_i(\phi,\alpha,\eta) = \frac{3}{2}\alpha\left[\frac{2}{3}\phi\alpha^2\eta^{-1} + \phi(1-\alpha^2) - (1-\alpha)^2\right] \qquad (A20)$$

$$\widehat{Q}_o(\phi,\alpha) = \phi - 1 + \frac{\phi}{2}\alpha(1+\alpha^2) + \alpha(1 - 3\alpha^+\alpha^2). \quad (A21)$$

[63] With the condition of conservation of volume ($Q_i + Q_o = 0$) the equation for the position of the interface is determined by the equation

$$\alpha^3\left(2\phi\eta^{-1} - 2\phi - 7\right) + 6\alpha^2 + \alpha(4\phi - 1) + 2\phi - 2 = 0. \qquad (A22)$$

[64] Note the similarity between $Q^*$ and $Q_s$. In equation (A10) the constant $\frac{\pi}{8}$ accounts for the cylindrical geometry whereas in equation (A19) the coefficient $\frac{2}{3}\frac{L}{A}$ accounts for the aspect ratio of the slot.

## Acknowledgments

## References

Allard, P., J. Carbonnelle, N. Mètrich, H. Loyer, and P. Zettwoog (1994), Sulphur output and magma degassing budget of Stromboli volcano, *Nature*, *368*, 326–329, doi:10.1038/368326a0.

Allard, P., M. Burton, and F. Mure (2005), Spectroscopic evidence for a lava fountain driven by previously accumulated magmatic gas, *Nature*, *433*, 407–410.

Arakeri, J. H., F. E. Avila, J. M. Dada, and R. O. Tovar (2000), Convection in a long vertical tube due to unstable stratification– A new type of turbulent flow?, *Curr. Sci.*, *79*(6), 859–866.

Arney, M., R. Bai, E. Guevara, D. Joseph, and K. Liu (1993), Friction factor and holdup studies for lubricated pipelining-I, *Int. J. Multiphase Flow*, *19*(6), 1061–1076.

Batchelor, G. (1967), *An Introduction to Fluid Dynamics*, 2nd ed., 615 pp., Cambridge Univ. Press, Cambridge, U. K.

Blake, S., S. Self, K. Sharma, and S. Sephton (2010), Sulfur release from the Columbia River Basalts and other flood lava eruptions constrained by a model of sulfide saturation, *Earth*

*Planet. Sci. Lett.*, *299*(3–4), 328–338, doi:10.1016/j. epsl.2010.09.013.

Bratsun, D. A., A. V. Zyuzgin, and G. F. Putin (2003), Non-linear dynamics and pattern formation in a vertical fluid layer heated form the side, *Int. J. Heat Fluid Flow*, *24*, 835–852.

Burton, M. R., H. Mader, and M. Polacci (2007a), The role of gas percolation in quiescent degassing of persistently active basaltic volcanoes, *Earth Planet. Sci. Lett.*, *264*, 46–60.

Burton, M. R., P. Allard, F. Murè, and A. La Spina (2007b), Magmatic gas composition reveals the source of Strombolian explosive activity, *Science*, *317*, 227–230.

Calder, E. S., A. J. L. Harris, P. Peña, E. Pilger, L. P. Flynn, G. Fuentealba, and H. Moreno (2004), Combined thermal and seismic analysis of the Villarrica volcano lava lake, Chile, *Rev. Geol. Chile*, *31*(2), 259–272.

Casertano, L. (1963), Activity of Villarrica volcano in the current century [in Spanish], *Bol. Univ. Chile*, *40*, 22–28, 48–54.

Cigolini, C., M. Laiolo, and S. Bertolino (2008), Probing Stromboli volcano from the mantle to paroxysmal eruptions, in *Dynamics of Crustal Magma Transfer, Storage and Differentiation*, edited by C. Annen and G. F. Zellmer, *Spec. Pap. Geol. Soc. Am.*, *304*, 33–70.

Corsaro, R. A., and M. Pompilio (2004), Dynamics of magmas at Mount Etna, in *Mt. Etna: Volcano Laboratory*, *Geophys. Mongr. Ser.*, edited by A. Bonaccoroso et al., vol. 143, pp. 91–110, AGU, Washington, D. C.

Costa, A., L. Caricchi, and N. Bagdassarov (2009), A model for the rheology of particle-bearing suspensions and partially molten rocks, *Geochem. Geophys. Geosyst.*, *10*, Q03010, doi:10.1029/2008GC002138.

Debacq, M., J. Hulin, D. Salin, B. Perrin, and E. Hinch (2003), Buoyant mixing of miscible fluids of varying viscosities in vertical tubes, *Phys. Fluids*, *15*(12), 3846–3855.

Gay, E., P. Nelson, and W. Armstrong (1969), Flow properties of suspensions with high solids concentration, *AIChE J.*, *15*, 815–822.

Gerlach, T. M. (1986), Exsolution of $H_2O$, $CO_2$, and S during eruptive episodes at Kilauea volcano, Hawaii, *J. Geophys. Res.*, *91*, 12,177–12,185.

Gerlach, T., H. Westrich, and R. Symonds (1996), Preeruption vapor in magma of the climactic Mount Pinatubo eruption: Source of the giant stratospheric sulfur dioxide cloud, in *Fire and Mud: Eruptions and Lahars of Mount Pinatubo, Philippines*, edited by C. Newhall and R. Punongbayan, pp. 415–433, Univ. of Wash. Press, Seattle.

Giordano, D., J. Russell, and D. Dingwell (2008), Viscosity of magmatic liquids: A model, *Earth Planet. Sci. Lett.*, *271*(1–4), 123–134, doi:10.1016/j.epsl.2008.03.038.

Hickox, C. E. (1971), Instability due to viscosity and density stratification in axisymmetric pipe flow, *Phys. Fluids*, *14*(2), 251–262.

Hui, H., and Y. Zhang (2007), Toward a general viscosity equation for natural anhydrous and hydrous silicate melts, *Geochim. Cosmochim. Acta*, *71*, 403–416.

Huppert, H. E., and M. A. Hallworth (2007), Bi-directional flows in constrained systems, *J. Fluid Mech.*, *578*, 95–112.

Ishibashi, H. (2009), Non-newtonian behavior of plagioclase-bearing basaltic magma: Subliquidus viscosity measurement of the 1707 basalt of Fuji volcano, Japan, *J. Volcanol. Geotherm. Res.*, *181*(1–2), 78–88.

Ishibashi, H., and H. Sato (2007), Viscosity measurements of subliquidus magmas: Alkali olivine basalt from the Higashi-Matsuura district, Southwest Japan, *J. Volcanol. Geotherm. Res.*, *160*(3–4), 223–238.

Jaluria, Y. (2003), Natural convection, in *Heat Transfer Handbook*, edited by A. Bejan and A. D. Kraus, pp. 525–571, Wiley, New York.

Jin, Y. Y., and C. F. Chen (1996), Natural convection of high Prandtl number fluids with variable viscosity in a vertical slot, *Int. J. Heat Fluid Flow*, *39*(13), 2663–2670.

Joseph, D. D., and Y. Y. Renardy (1993a), *Fundamentals of Two-Fluid Dynamics. Part I: Mathematical Theory and Applications*, *Interdiscip. Appl. Math.*, vol. 3, 473 pp., Springer, New York.

Joseph, D. D., and Y. Y. Renardy (1993b), *Fundamentals of Two-Fluid Dynamics. Part II: Lubricated Transport, Drops and Miscible Liquids*, *Interdiscip. Appl. Math.*, vol. 4, 453 pp., Springer, New York.

Kazahaya, K., H. Shinohara, and G. Saito (1994), Excessive degassing of Izu-Oshima volcano: magma convection in a conduit, *Bull. Volcanol.*, *56*, 207–216.

Lavallée, Y., K.-U. Hess, B. Cordonnier, and D. B. Dingwell (2007), Non-newtonian rheological law for highly crystalline dome lavas, *Geology*, *35*(9), 843–846.

Locke, C. A., H. Rymer, and J. Cassidy (2003), Magma transfer processes at persistently active volcanoes: insights from gravity observations, *J. Volcanol. Geotherm. Res.*, *127*, 73–86.

Mandal, T. K., D. P. Chakrabarti, and G. Das (2007), Oil water flow through different diameter pipes: Similarities and differences, *Chem. Eng. Res. Des.*, *85*(A8), 1123–1128, doi:10.1205/cherd0603.

Marsh, B. (1981), On the crystallinity, probability of occurrence, and rheology of lava and magma, *Contrib. Mineral. Petrol.*, *78*, 85–98.

Mattia, M., M. Rossi, F. Guglielmino, M. Aloisi, and Y. Bock (2004), The shallow plumbing system of Stromboli Island as imaged from 1 Hz instantaneous GPS positions, *Geophys. Res. Lett.*, *31*, L24610, doi:10.1029/2004GL021281.

McBirney, A., and T. Murase (1984), Rheological properties of magmas, *Annu. Rev. Earth Planet. Sci.*, *12*, 337–357.

Oppenheimer, C., A. S. Lomakina, P. R. Kyle, N. G. Kingsbury, and M. Boichu (2009), Pulsatory magma supply to a phonolite lava lake, *Earth Planet. Sci. Lett.*, *284*, 392–398.

Palma, J. L., E. S. Calder, D. Basualto, S. Blake, and D. A. Rothery (2008), Correlations between $SO_2$ flux, seismicity, and outgassing activity at the open vent of Villarrica volcano, Chile, *J. Geophys. Res.*, *113*, B10201, doi:10.1029/2008JB005577.

Petit-Breuilh, M. (1994), Contribución al conocimiento de la cronología eruptiva del volcán Villarrica (39–25°S) 1558–1985, *Rev. Frontera*, *13*, 71–99.

Pinkerton, H., and R. J. Stevenson (1992), Methods of determining the rheological properties of magmas at sub-liquidus temperatures, *J. Volcanol. Geotherm. Res.*, *53*, 47–66.

Ripepe, M., E. Marchetti, G. Ulivieri, A. Harris, J. Dehn, M. Burton, T. Caltabiano, and G. Salerno (2005), Effusive to explosive transition during the 2003 eruption of Stromboli volcano, *Geology*, *33*(5), 341–344, doi:10.1130/G21173.1.

Self, S., S. Blake, K. Sharma, M. Widdowson, and S. Sephton (2008), Sulfur and chlorine in Late Cretaceous Deccan magmas and eruptive gas release, *Science*, *319*(5870), 1654–1657.

Shinohara, H. (2008), Excess degassing from volcanoes and its role on eruptive and intrusive activity, *Rev. Geophys.*, *46*, RG4005, doi:10.1029/2007RG000244.

Shinohara, H., and J. Witter (2005), Volcanic gases emitted during mild strombolian activity of Villarrica volcano, Chile, *Geophys. Res. Lett.*, *32*, L20308, doi:10.1029/2005GL024131.

Sparks, R. S. J. (2003), Dynamics of magma degassing, in *Volcanic Degassing*, edited by C. Oppenheimer, D. Pyle, and J. Barclay, *Spec. Pap. Geol. Soc. Am.*, 5–22.

Spera, F. J. (2000), Physical properties of magma, in *Encyclopedia of Volcanoes*, edited by H. Sigurdsson et al., pp. 171–190, Academic, San Diego, Calif.

Stevenson, D. S., and S. Blake (1998), Modelling the dynamics and thermodynamics of volcanic degassing, *Bull. Volcanol.*, 60, 307–317.

Stix, J. (2007), Stability and instability of quiescently active volcanoes: the case of Masaya, Nicaragua, *Geology*, 35(6), 535–538.

Symonds, R. B., W. I. Rose, G. J. Bluth, and T. Gerlach (1994), Volcanic-gas studies: methods, results, and applications, in *Volatiles in Magmas, Reviews in Mineralogy*, vol. 30, edited by M. R. Carrol and J. Holloway, chap. 1, pp. 1–66, Mineral. Soc. of Am., Chantilly, Va.

Turcotte, D. (1987), Physics of magma segregation processes, in *Magmatic Processes: Physicochemical Principles*, edited by B. O. Mysen, *Spec. Publ. Geochem. Soc.*, 1, 69–74.

Wallace, P., and A. Anderson (1998), Effect of eruption and lava drainback on the $H_2O$ contents of basaltic magmas at Kilauea volcano, *Bull. Volcanol.*, 59, 327–344.

Witter, J. B., V. C. Kress, P. Delmelle, and J. Stix (2004), Volatile degassing, petrology, and magma dynamics of the Villarrica Lava Lake, Southern Chile, *J. Volcanol. Geotherm. Res.*, 134, 303–337.